

## Research paper

# Diagenesis and reservoir quality of sandstones with ancient “deep” incursion of meteoric freshwater—An example in the Nanpu Sag, Bohai Bay Basin, East China

Guanghui Yuan <sup>a, b, \*</sup>, Yingchang Cao <sup>a, b, \*\*</sup>, Yongchao Zhang <sup>c</sup>, Jon Gluyas <sup>d</sup><sup>a</sup> School of Geosciences, China University of Petroleum, Qingdao, 266580, China<sup>b</sup> Laboratory for Marine Mineral Resources, Qingdao National Laboratory for Marine Science and Technology, Qingdao, 266071, China<sup>c</sup> PetroChina Jidong Oilfield Company, Tangshan 063004, Hebei, China<sup>d</sup> Department of Earth Sciences, Durham University, Durham, DH1 3LE, UK

## ARTICLE INFO

## Article history:

Received 29 November 2016

Received in revised form

18 February 2017

Accepted 23 February 2017

Available online 24 February 2017

## Keywords:

Meteoric-water diagenesis

Freshwater leaching

Enhanced secondary pores

Open geochemical system

Uplift

Nanpu sag

## ABSTRACT

An example of diagenesis and reservoir quality of buried sandstones with ancient incursion of meteoric freshwater is presented in this study. The interpretation is based on information including porosity and permeability, petrography, stable isotopic composition of authigenic minerals, homogenization temperatures ( $T_h$ ) of aqueous fluid inclusions (AFIs), and pore water chemistry. These sandstones, closely beneath or far from the regional unconformity formed during the late Paleogene period, are located in the thick Shahejie Formation in the Gaoliu area of Nanpu Sag, Bohai Bay Basin, East China. Early-diagenetic calcite cements were leached to form intergranular secondary pores without precipitation of late-diagenetic calcite cements in most sandstones. Feldspars were leached to form abundant intra-granular secondary pores, but with small amounts of concomitant secondary minerals including authigenic quartz and kaolinite. The mass imbalance between the amount of leached minerals and associated secondary minerals suggests that mineral leaching reactions occurred most likely in an open geochemical system, and diagenetic petrography textures suggest that advective flow dominated the transfer of solutes from leached feldspars and calcites. Low salinity and ion concentrations of present pore waters, and extensive water rock interactions suggest significant incursion of meteoric freshwater flux in the sandstones. Distances of the sandstones to the regional unconformity can reach up to 1800 m, while with significant uplift in the Gaoliu area, the burial depth of such sandstones (below sea level) can be less than 800–1000 m during the uplift and initial reburial stage. Significant uplift during the Oligocene period provided substantial hydraulic drive and widely developed faults served as favorable conduits for downward penetration of meteoric freshwater from the earth's surface (unconformity) to these sandstone beds. Extensive feldspar leaching has been occurring since the uplift period. Coupled high  $T_h$  (95–115 °C) of AFI and low  $\delta^{18}O_{(SMOW)}$  values (+17~+20‰) within the quartz overgrowths show that quartz cementation occurred in the presence of diagenetic modified meteoric freshwater with  $\delta^{18}O_{(SMOW)}$  values of -7~-2‰, indicating that authigenic quartz only have been formed during the late reburial stage when meteoric fresh water penetration slowed down. Secondary pores in thin sections and tested porosity suggest that meteoric freshwater leaching of feldspars and calcite minerals generated approximately 7–10% enhanced secondary porosity in these sandstones. Meteoric freshwater leaching reactions cannot be ignored in similar sandstones that located deep beneath the unconformity, with great uplift moving these sandstones above or close to sea level and with faults connecting the earth's surface with the sandstone beds.

© 2017 Elsevier Ltd. All rights reserved.

\* Corresponding author. School of Geosciences, China University of Petroleum, Qingdao, 266580, China.

\*\* Corresponding author. School of Geosciences, China University of Petroleum, Qingdao, 266580, China; Laboratory for Marine Mineral Resources, Qingdao National Laboratory for Marine Science and Technology, Qingdao, 266071, China.

E-mail addresses: [yuan.guanghui86@gmail.com](mailto:yuan.guanghui86@gmail.com) (G. Yuan), [caoych@upc.edu.cn](mailto:caoych@upc.edu.cn) (Y. Cao).

## 1. Introduction

Secondary porosity, formed by dissolution of detrital grains and authigenic cements, is an important contributor to reservoir quality in buried sandstones (Dutton and Loucks, 2010; Franca et al., 2003;

Molenaar et al., 2015; Wilkinson et al., 2014). Secondary pores in rocks are generally formed by meteoric freshwater leaching at shallow depth after deposition or closely beneath unconformity during uplift stage (Baruch et al., 2015; Bjørlykke and Jahren, 2012; Emery et al., 1990; França et al., 2003), by deep burial leaching induced by acids generated from kerogen maturation within source rocks (Schmidt and McDonald, 1979; Surdam et al., 1984; Yuan et al., 2015a), or by deep hot water (Taylor and Land, 1996). Most meteoric diagenetic alterations have been suggested to occur closely beneath unconformities (Emery et al., 1990; Huang et al., 2003) or at burial depth less than a few hundred meters (Bjørlykke and Jahren, 2012; Bjørlykke and Aagaard, 1992; Mansurbeg et al., 2006).

França et al. (2003) reported an example of meteoric water leaching in Botucatu sandstones from outcrops to a burial depth of 1000–1500 m, but with petrographic evidence of mineral dissolution mainly occurring in sandstones shallower than 250 m. Gluyas et al. (1997) presented finding concerning the incursion of meteoric water in buried Rotliegend sandstones during an uplift period (Gluyas et al., 1997). No diagenetic mineral assemblages (with mass imbalance between leached minerals and associated secondary minerals) representing an open geochemical system, however, were reported in the study. Up to the present day, there are a few examples documenting burial leaching reactions induced by “deep” incursion (>1000–1500 m) of meteoric freshwater into buried sandstones in layers of rock with thickness up to 1–2 km (França et al., 2003).

The Nanpu Sag in Bohai Bay Basin is an important oil and gas producing province in East China (Guo et al., 2013; Zhu et al., 2011). The Shahejie Formation in the Gaoliu area of the Nanpu Sag is an important hydrocarbon producing layers, with present burial depth reaching up to 3500–4000 m below sea level (Zhang et al., 2008). On top of the Shahejie Formation or overlying upper Dongying Formation is a regional unconformity formed in the end Paleogene period (Guo et al., 2013). The Shahejie Formation in the Gaoliu area is very thick, and the distance between the unconformity and sandstones in the lower Shahejie Formation is up to 1500–1800 m (Yuan et al., 2015b).

Sandstones in the thick Shahejie Formation have experienced very extensive leaching of detrital feldspars with re-precipitation of only few secondary minerals (authigenic kaolinite, quartz) (Yuan et al., 2015b; Zhang et al., 2008). After extensive diagenesis, the present pore waters in the sandstone reservoirs, however, are characterized by low salinity, low ion concentrations and negative hydrocarbon isotopic composition, suggesting the impact of meteoric freshwater on these sandstones in geologic time (Yuan et al., 2015b; Zhang et al., 2008). But there is still study suggests that organic acids from kerogen maturation dominated the mineral dissolution in the sandstones (Gao et al., 2016). Thus, detailed evolution history of the diagenetic reactions and the relevant paleo-fluids in the Shahejie sandstones with freshwater incursion and the reservoir quality evolution of such sandstones should be thoroughly studied with a combination of the published data and some new data. With simple burial history (burial-uplift-reburial), high quality 3D seismic data, abundant drilling wells and core samples, and other geological information, the thick Shahejie Formation in the Gaoliu area is an ideal medium for studying diagenesis and reservoir quality evolution of sandstones with impact of ancient meteoric freshwater flux.

By using a combination of porosity and permeability, petrography, stable isotopic compositions of authigenic minerals,  $T_h$  of aqueous fluid inclusions (AFI) and pore water chemistry, the objectives of this paper are: (1) to investigate the diagenetic features and reconstruct the detailed diagenetic sequences in the sandstones of the thick Shahejie Formation in the Gaoliu area; (2) to

study the paleo-fluid evolution history and identify the ancient “deep” incursion of meteoric freshwater into the sandstones; and (3) to verify that meteoric-leaching can form enhanced secondary pores to improve reservoir quality. This study presented how to identify incursion of meteoric freshwater in surface sandstones, and the meteoric leaching model proposed in this study is of great significance for exploration of deeply buried sandstones with great uplift in geological time.

## 2. Geological background

The Nanpu (NP) Sag, a subunit of Bohai Bay Basin, is located on the eastern coast of China and covers approximately 2462 km<sup>2</sup>. It is a rift lacustrine basin developed from the Late Jurassic to the early Cenozoic on the basement of the North China platform. The Nanpu Sag is further subdivided into 12 secondary structural units (Fig. 1A) (Guo et al., 2013). The Gaoliu area (including the Gaoshangpu structural belt and the Liuzan structural belt) at the northern part of the Nanpu sag was bounded by the Xi'nanzhuang growth fault, the Baigezhuang growth fault and the Gaoliu growth fault (Fig. 1). The Gaoliu area, with an area of approximately 200 km<sup>2</sup> (Zhang et al., 2008), is the objective area of this study.

From base to top, the sediments deposited in the Nanpu Sag are represented by the Shahejie (Es), Dongying (Ed), Guantao (Ng), Minghuazhen (Nm), and Pingyuan (Q) formations (Fig. 1C; Fig. 2) (Guo et al., 2013; Yuan et al., 2015b). The Shahejie Formation contains high quality source rocks and reservoir rocks (Zhu et al., 2011), and is divided into three members as Es3, Es2, and Es1 from base to top (Fig. 2). The Es3 member includes five sub-members of Es<sub>3</sub><sup>5</sup> - Es<sub>3</sub><sup>1</sup> (from base to top). The Dongying Formation is divided into three members including the Ed3, Ed2 and Ed1 (from base to top).

Tectonic evolutionary history of the Nanpu Sag has been analyzed in detail using 3D seismic data and drilling wells (Zhou, 2000). Regional uplift in the late Oligocene (approximately 27 Ma–23 Ma) contributed to the formation of a regional unconformity between the Ng Formation and the underlying layers. During this uplift stage, the Gaoliu growth fault between the Gaoliu area and the Liunan sub-sag led to a significant uplift difference between the Gaoliu area and other tectonic zones (Fig. 1C) (Guo et al., 2013). In the Gaoliu area, Ed1, Ed2 and the upper part of Ed3 were heavily eroded, leaving only the lower Ed3 preserved locally (Fig. 2A); while only the upper part of Ed1 was eroded in other tectonic zones (eg. Liunan subsag) (Fig. 2B) (Guo et al., 2013). In the Gaoliu area, the Es1 member, Es<sub>1</sub><sup>1</sup>, Es<sub>1</sub><sup>2</sup>, Es<sub>1</sub><sup>3</sup> and Es<sub>1</sub><sup>5</sup> sub-members consist mainly of gray, purple-gray, brownish, and greenish mudstones and interbedded fan delta sandstones deposited in shallow lacustrine environments. The Es<sub>1</sub><sup>4</sup> sub-member consists mainly of dark-gray oil shale, dark-gray mudstones, calcareous mudstones deposited in a semi-deep and deep lacustrine environment and gray mudstones with interbedded deltaic fan sandstones deposited in a shallow lacustrine environment (Fig. 2A) (Guo et al., 2013; Yuan et al., 2015b). The Es2 member consists mainly of brownish mudstones and interbedded sandstones deposited in fluvial systems or alluvial fans.

The present-day geothermal gradient in the Gaoliu area is around 32 °C/km, with an average earth surface temperature of 14 °C. The burial and thermal history of the NP sag has been analyzed in detail with data from exploration and production wells using PetroMod 1D software (Fig. 2) (Guo et al., 2013). Maximum burial depth and temperature of the sandstones in the Shahejie Formation occur today. Due to tectonic differences, the burial and thermal history of sediments in the Gaoliu area (Fig. 2A) varies significantly from that of the sediments in the Liunan subsag (Fig. 2B) and other structural belts. During the late Oligocene uplift period, the thickness of eroded strata is up to 500–600 m in the

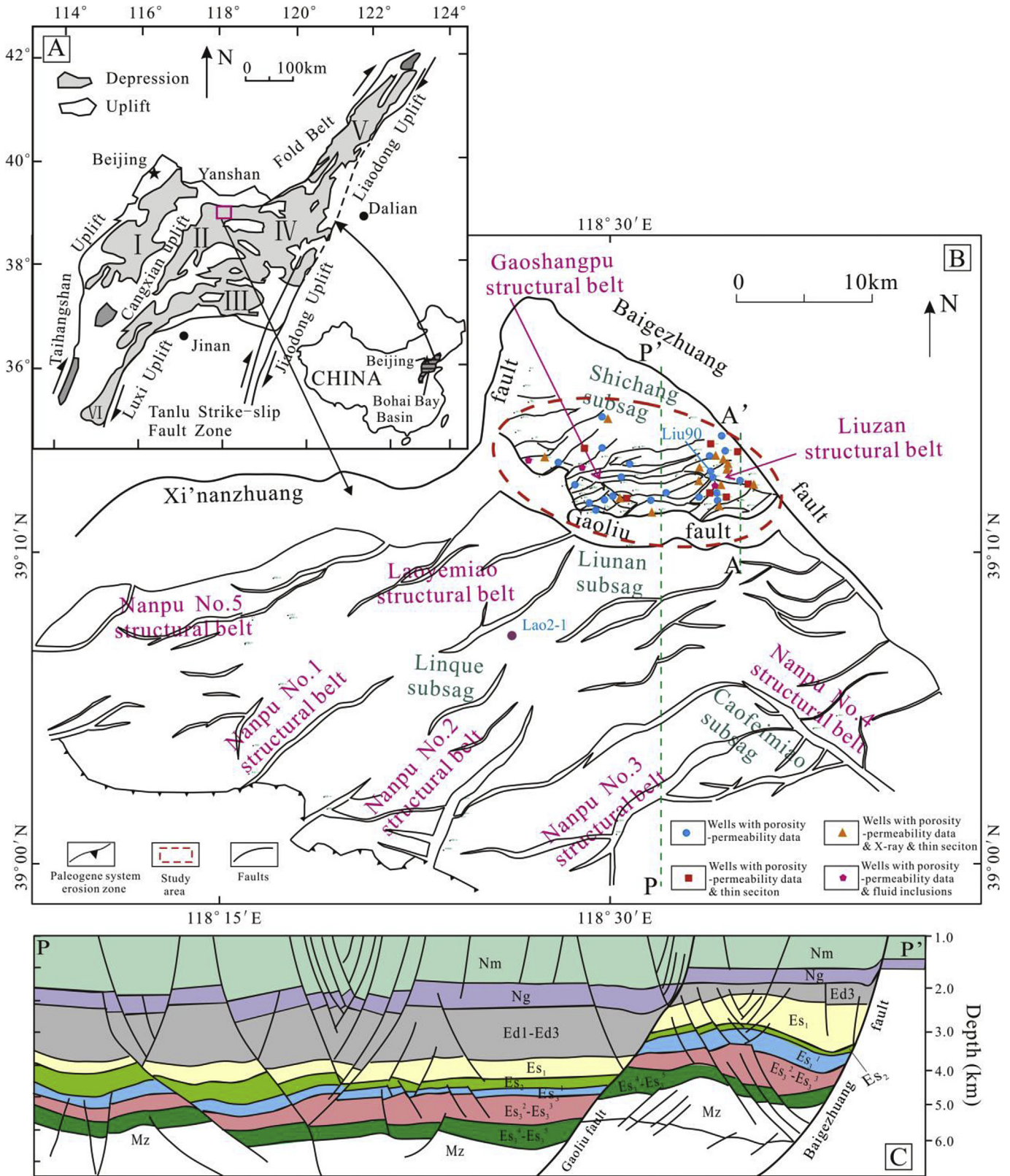


**Fig. 1.** A-Location map of the Gaoliu area (Gaoshangpu structural belt and Liuzan structural belt) in the Nanpu Sag, modified from Yuan et al (2015b). B-Cross-section (00' in Fig. 1A) of the Nanpu Sag showing the various tectonic-structural zones and strata in different zones, Modified from Guo et al. (2013).

Gaoliu area, but less than 200–300 m in other structural belts in the Nanpu Sag, as estimated based on acoustic travel time logging (AC) calculations (Guo et al., 2013).

The basin-subsidence-controlling Xi'nanzhaung growth fault and Baigezhuang growth fault initiated their activity from the early Paleogene period, and the Gaoliu growth fault initiated its activity

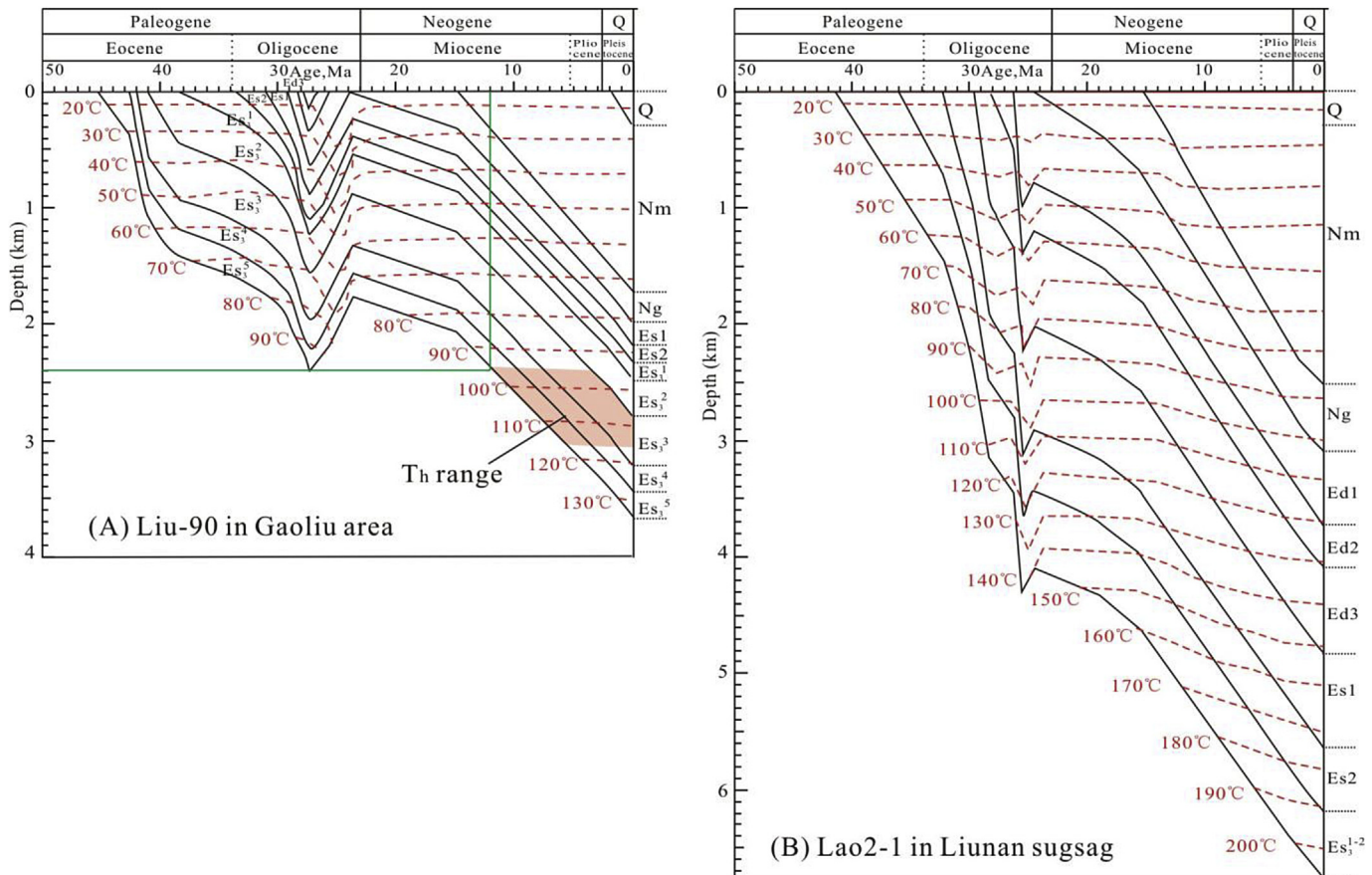


Fig. 2. Burial and thermal history of well Liu-90 (A) in the Gaoliu area and well Lao2-1 (B) in Liunan subsag (modified from Guo et al., 2013). Shaded area in Fig. 2A represents the  $T_h$  data range of aqueous fluid inclusion in quartz overgrowths.

from the early Oligocene period. The three faults continued activity until the end of the Pliocene period (Dong et al., 2008; Li et al., 2010; Zhou, 2000) (Fig. 1). These three primary faults were joined by multiple synthetic and antithetic faults that formed during the late Oligocene period to early Neogene period, and these additional faults were active to the end of Pliocene period (Li et al., 2010; Zhou, 2000). In the seismic section, these faults can be identified to connect the deeply buried Shahejie Formation to shallow strata (Fig. 3) (Yuan et al., 2015b).

### 3. Database and methods

Reservoir porosity and permeability data of 3368 standard core plugs (2.5 cm diameter) and chemistry data of 242 formation water samples from the Shahejie sandstone reservoirs were collected from Nanpu Oilfield Company. The porosity and permeability were analyzed using CMS<sup>tm</sup>-300 Core Measurement system with  $N_2$  and a confining pressure of 6 Mpa. The formation water samples were obtained at well heat during drill-stem testing or formation testing from oil or water intervals. The water samples were not collected until the fluid production and the  $Cl^-$  concentration reached stable. The collected formation water samples were preserved in sealed bottles before analysis. The chemistry data were tested in two weeks using a 930 Compact ion chromatograph.

One hundred and twenty blue epoxy resin-impregnated thin sections and 40 scanning electron microscope (SEM) samples from the Shahejie sandstone cores of 17 wells were analyzed for sandstone petrography, diagenesis and pores, using optical, reflected, and cathodoluminescence (CL) microscopy and a Coxem-30<sup>plus</sup>

SEM facility. Oil in the core samples was removed first using alcohol-benzene compound. Impregnation was undertaken in a vacuum to remove gas from the samples; samples were dried at 50 °C and the blue epoxy was cured at 60 °C and injected into the samples with a pressure of 50 Mpa. After polishing to 30  $\mu m$  thickness, the thin sections were partly stained with Alizarin Red and K-ferricyanide for carbonate mineral identification. Optical and reflected identification were conducted using a Zeiss (Axioplan 2 imaging) microscope. CL images were collected using a CAM-BRIDGE CL8200 MK5 detector on the Zeiss microscope with an accelerating voltage of 15 kV. Point-counts were performed on the thin sections for the detrital compositions, and the quantitative content of secondary pores and authigenic cements was conducted using the image analysis method described by Yuan et al. (2015c). SEM image observation was undertaken on gold coated, freshly broken samples glued onto aluminum stubs. The Coxem-30<sup>plus</sup> SEM was attached with a Bruker Energy Dispersive X-ray analysis system (EDX) (XFlasher Detector 430-M), which allows analysis at a specific spot of about 1  $\mu m$  diameter or collects emissions from a specific line on the screen or the whole screen area.

Based on the examination of hundreds of these thin sections, six core plugs with development of some quartz overgrowths were picked out to make 100  $\mu m$  thickness doubly polished sections for fluid inclusion and  $\delta^{18}O$  composition analysis. The six sandstone samples were collected from each of six drilling cores, with burial depths ranging from 2800 m to 4000 m. UV light was used to identify aqueous fluid inclusions (AFI). Microthermometry of AFI was conducted using a calibrated Linkam TH-600 stage. The homogenization temperature ( $T_h$ ) was obtained by cycling.  $T_h$

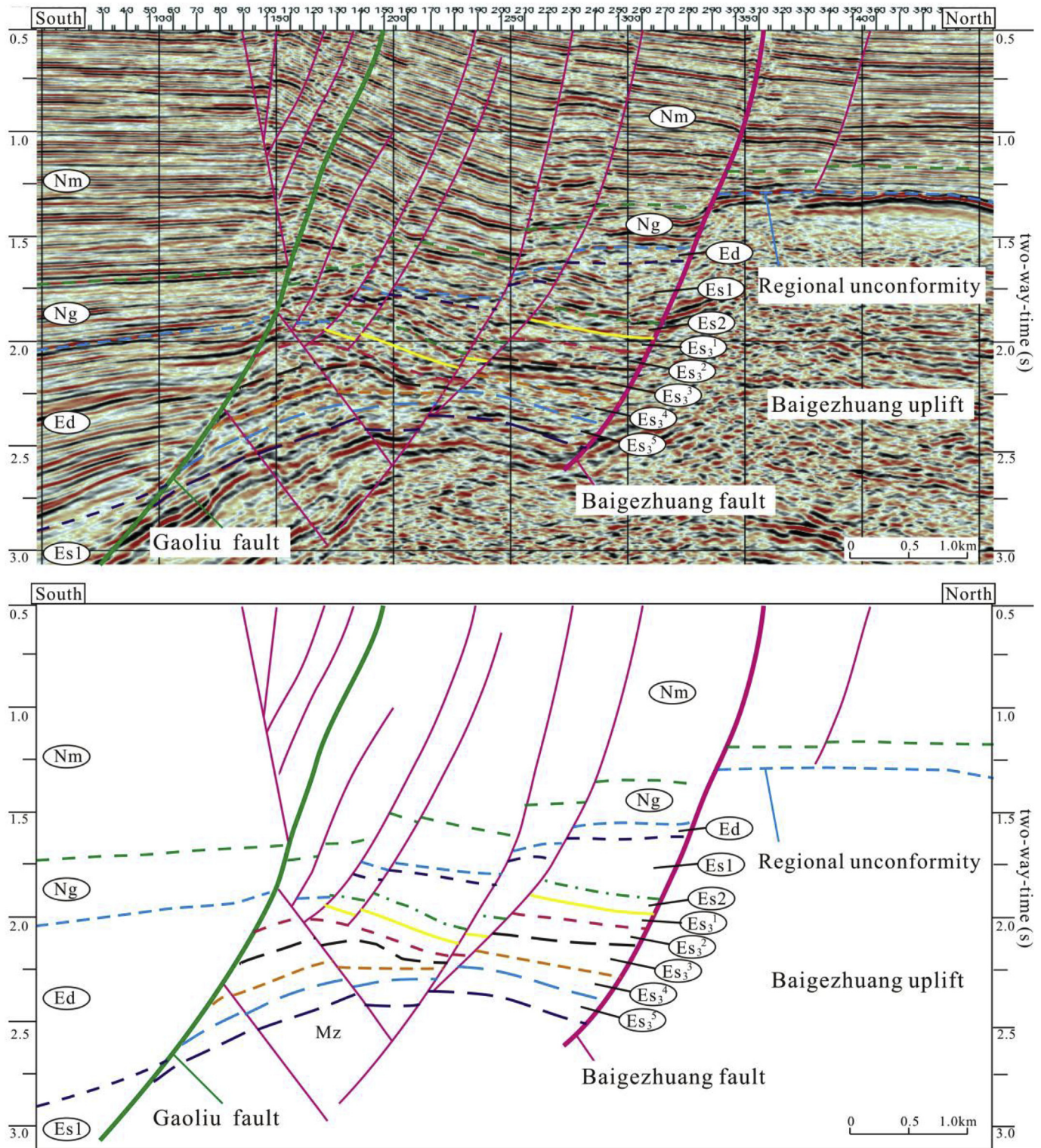


Fig. 3. Seismic section showing faults developed in the Gaoliu area (north-south cross section A'A in Fig. 1A).

measurements were determined using a heating rate of 10 °C/min when temperature was lower than 70 °C and a rate of 5 °C/min when temperature exceeded 70 °C (Chen et al., 2016). The measured temperature precision for  $T_h$  is  $\pm 1$  °C.

Areas of four of the six thin sections with some thick quartz overgrowths (>25  $\mu\text{m}$  wide) were identified using optical and

reflected light microscopy. These areas were then cored out from the doubly polished thin sections, and then mounted into two resin blocks alongside NBS-28 standard quartz grains with known  $\delta^{18}\text{O}$  value. Micrographs of these three specimen blocks were, as mentioned above, captured with optical, reflected and cathodoluminescence (CL) microscopy to select ion microprobe spots.

In situ secondary ion mass spectrometry (SIMS) oxygen isotopic composition analysis of detrital quartz and quartz overgrowths in 4 sandstone samples was performed using a CAMECA IMS-1280 ion microprobe with an approximately 15  $\mu\text{m}$  diameter beam at the institute of Geology and Geophysics, Chinese Academy of Sciences (IGGCAS) in Beijing. The analytical procedures used were similar to those reported by Li et al., 2013. Samples after analysis were examined again using optical and reflected light microscopy to identify the location of craters, and CL was used to identify the phases of the quartz overgrowths that had been tested. The internal precision of  $\delta^{18}\text{O}$  is ca 0.2‰ (2 standard deviations, 2SD) from 20 cycles of measurements (Li et al., 2012). The reproducibility of  $\delta^{18}\text{O}$  by repeated measurements of standard quartz in this study averaged 0.3‰ (2SD).

Based on petrological studies, 10 organic matter-free sandstone samples were selected for analysis of the carbon and oxygen stable isotope composition in the carbonate cements. Tightly cemented sandstones were disaggregated with a hammer and then crushed in a mortar; porous sandstones were disaggregated using the freezing-heating technique to avoid breaking detrital carbonate grains (Wang et al., 2005). The disaggregated samples were then sieved to pass through a 200 mesh sieve (75  $\mu\text{m}$ ) to get the powder. This sample preparation method reduces the possibility of sampling unwanted detrital carbonates. Isotopic data were obtained using Thermo-Finnigan MAT 253 IRMS online with Gas BenchII in Durham University (Yuan et al., 2015c).  $\delta^{13}\text{C}$  and  $\delta^{18}\text{O}$  values were determined on the  $\text{CO}_2$  liberated from carbonate cements samples and the LAEAC01 standard that were dissolved by 100%  $\text{H}_3\text{PO}_4$  at 50 °C. Isotopic composition of  $\text{CO}_2$  is reported in units of ‰ relative to  $P_{\text{EE}}$  Dee Belemnite (V-PDB). Replicate analysis is reproducible to  $\pm 0.1\text{‰}$  for both  $\delta^{13}\text{C}$  and  $\delta^{18}\text{O}$  (Yuan et al., 2015c).

## 4. Results

### 4.1. Porosity and permeability

The Shahejie sandstones in the Gaoliu area have a wide range of porosity from 2.3% to 30% and permeability from 0.007 mD to 4139 mD (measured over the depth interval 2000 m–4000 m). In general,

the porosity and permeability of the Shahejie sandstones decrease but slightly as the burial depth increases from 2000 m to 4000 m. Reservoirs buried deeper than 3500 m can even host porosity up to 20% and permeability up to 100–1000 mD. Medium-coarse grained sandstones and pebbly sandstones have the highest porosity (2.9–28.8% and an average of 16.1%) and permeability (0.01–4135 mD and an average of 120 mD) (Fig. 4A1, A2), followed by fine-grained sandstones with moderate porosity (2.36–30.1% and an average of 14.5%) and permeability (0.007–4139 mD and an average of 79 mD) (Fig. 4B1, B2). Siltstones and shaly sandstones have the lowest porosity (3.2–20.8% and an average of 9.7%) and permeability (0.01–6.84 mD and an average of 0.6 mD) (Fig. 4C1, C2).

### 4.2. Sandstone petrography: detrital mineralogy

The Shahejie sandstones in the Gaoliu area are fine-to coarse-grained. The sandstones are generally texturally immature. Sorting ranges from poor to moderate sorted and roundness of the detrital grains varies from subangular to sub-rounded. Analyzed medium-to coarse-grained sandstones and pebbly sandstones in this study are clean, moderate-sorted lithic arkoses and feldspathic litharenites, compositionally immature with an average framework composition of  $\text{Q}_{30}\text{F}_{34}\text{L}_{36}$ , and less than 1% detrital clays (Table 1).

### 4.3. Sandstone petrography: diagenetic mineralogy

Authigenic minerals in the sandstones consist mainly of carbonate cements, kaolinite and quartz. The authigenic quartz and kaolinite are usually associated with leached feldspars (Figs. 5–7).

#### 4.3.1. Feldspar diagenesis

In the low porosity sandstone samples with large amounts of early-diagenetic carbonate cement (Fig. 7A), leached feldspars, authigenic quartz and clays are almost absent. While porous sandstones commonly contain many feldspar-hosted pores with small quantities of authigenic kaolinite and quartz (Fig. 5). Feldspar diagenesis significantly altered the composition of the sandstones, many feldspars, including mainly detrital K-feldspar grains and K-feldspar in rock fragments were identified as partially to fully

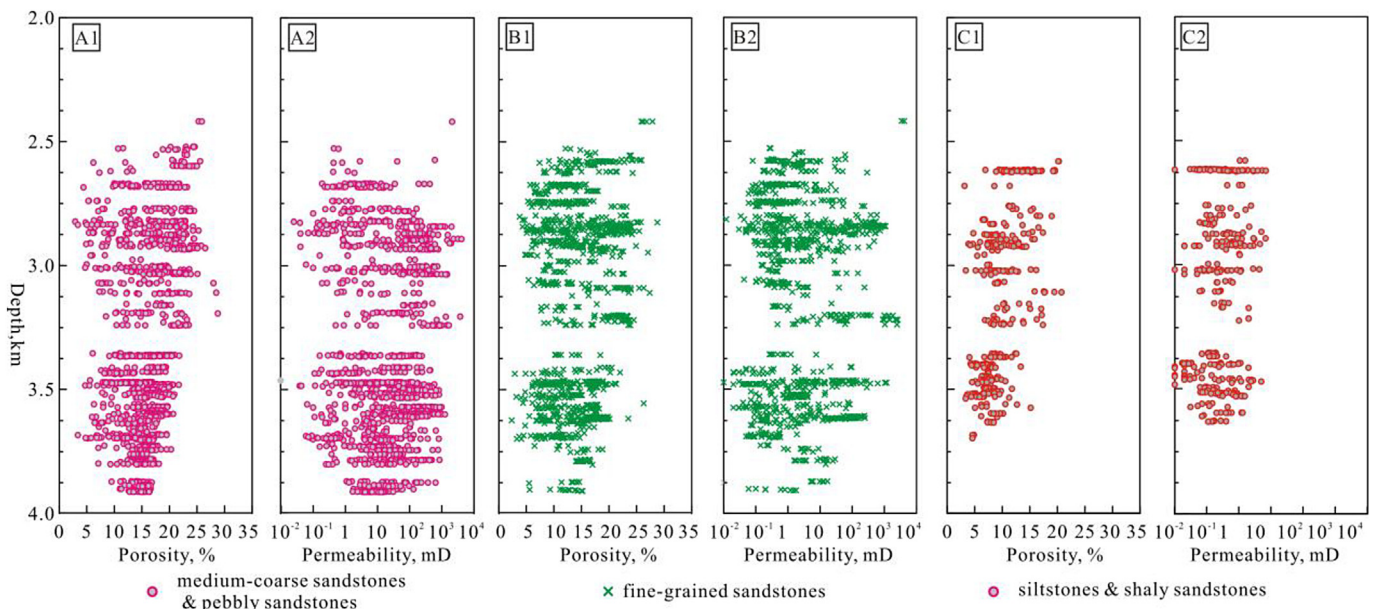


Fig. 4. Vertical distribution of core porosity and permeability of different sandstones in the Shahejie Formation in the Gaoliu area, Nanpu Sag.

**Table 1**  
Average thin-section compositions from optical point counting and quantitative image analysis.

Borehole	TVD, m	Distances to unconformity, m	n	Quartz, %	K-feldspar, %	Plagioclase, %	Rock fragment, %	Carbonate cement, %	Detrital clay, %	Authigenic kaolinite, %	QOF, %	Intragranular secondary pores in feldspars, %	Intergranular pores, %	Core plug porosity, %
Gao81	2722–2784	719–781	3	23–26	15–22	12–28	325–35	0–12	0.1–0.5	0–0.5	0–0.01	0.5–3	2–18	12–30.7
Gao5	3180–3242	1154–1216	11	29–35	8–16	15–27	29–44	0–25	0.1–10	0–0.2	0–0.02	0.2–4	0–10	8.8–23.9
Gao8x1	3813–3830	1567–1584	11	26–37	19–25	10–13	32–44	0.2–28	1.0–3.0	0–3.5	0	0–0.5	0	5.8–13.8
Gao13	3478–3523	1374–1419	6	24–28	10–15	20–21	37–43	0–2.5	0.2–3	0.2–2	0–0.05	2–3.5	0.2–3	14.5–19.7
Gao23	3560–3597	1595–1632	5	23–26	15–19	20–28	31–42	0–0.5	0.1–0.5	0.1–0.2	0.1–0.3	2.5–5	0.5–3	15.1–20.4
Gao3106	3570–3916	1487–1833	7	23–30	12–20	19–28	31–35	0.1–20	0.1–0.5	0–0.1	0–0.05	0–3	0–7	3.5–19
Liu1-3	2959–2961	907–909	3	25–28	18–26	12–14	32–45	0–0.5	2–3	0.5–2	0.03–0.05	0.5–1	3–7	23.6–26.5
Liu3-3	2957–3073	662–778	4	25–40	10–20	13–15	26–47	0–0.5	0.2–10	0–0.2	0–0.5	0–1	0–2	7–14
Liu12-2	3719–3726	1659–1666	7	25–32	15–20	18–23	33–39	0–5	0–10	0.2–2.5	0–0.05	0.3–2.5	0–1.2	–
Liu15	2624–3521	446–1343	10	28–35	12–18	13–22	30–40	0.2–10	0.1–15	0–1.5	0–0.05	0.05–4	0–8	5.4–32.8
Liu24	2621–3027	449–855	5	28–41	26–35	10–16	8–34	0.2–5	0.2–0.3	0.05–0.1	0–0.1	0.5–1	4–6	15.9–20
Liu160x1	3475–3478	1421–1424	11	18–23	20–22	9–12	44–51	0–4	0.2–12	0–0.2	0–0.05	0–5	0–6	9.6–19.1
Liu68x1	3334–3818	749–1233	7	26–35	15–17	12–18	35–41	0.5–3	0.1–4	0.05–2	0.01–1.5	0.5–2	0–1	–
Liu124x1	2819–3002	648–831	13	26–35	11–21	10–21	27–42	0.2–15	0.2–5	0–0.2	0–0.02	0.2–4	0–10	16.8–17.2
Liu158x1	3310–3361	1424–1475	6	26–31	20–30	10–12	22–43	0–2	0.1–3	0.01–1	0–0.3	0.2–4	1.5–4	9.7–16.8
Liu160x1	2574–2862	688–977	6	32–35	14–20	16–20	29–36	0–20	1–18	0–0.2	0–0.01	0–1	0–10	–
LiuShen11	2622–2633	430–441	5	30–46	15–25	8–10	28–37	0–25	0.2–15	0–0.1	0–0.1	0–2	0–10	–

–, not detected, QOF-quartz overgrowths.

Intergranular pores including primary pores and secondary pores formed by calcite leaching.

dissolved (Fig. 5). Monocrystalline and polycrystalline feldspar grains may be fully dissolved (Fig. 5A, D), though most feldspars are partly dissolved (Fig. 5 C, E). The internal fabric of the feldspar is still recognizable by intricate structures consisting of inherited minerals and secondary pores after the former cleavage or twinning or perthitic structures (Fig. 5 C, E). The partial dissolution may be due either to the variety of compositions or limited leaching, and the remnants can be used to identify dissolution texture. Some detrital plagioclase grains were identified to be partially leached, but not commonly. In most cases, the intragranular secondary pores after detrital feldspars and intergranular primary pores are not filled with newly formed minerals, which is different with most other buried sandstones (Bjørlykke and Jahren, 2012; Chuhan et al., 2001; Molenaar et al., 2015). The amount of feldspar secondary pores can reach up to 4–5% in the thin sections (Table 1).

Authigenic quartz was identified in the thin sections of some core samples buried deeper than 2800 m, amounting to less than 0.1% of the total rock (Table 1). Authigenic quartz occurs as syntaxial quartz overgrowths (Fig. 5G and H) or small microcrystalline quartz (Fig. 6A). The thickness of these quartz overgrowths ranges mainly from 2 μm to 30 μm, and the size of the quartz crystals is generally less than 15 μm. Quartz overgrowths can be easily identified by dust rims or fluid inclusions located at the grain-overgrowth boundary, while microcrystalline quartz crystals can be easily identified in SEM images.

Authigenic kaolinite can be identified occasionally in thin sections and SEM images of some samples, with an amount less than 0.5% in most samples (Table 1). These kaolinite occurs mainly as vermicular aggregates, anhedral and pseudohexagonal plates filling primary pores and a few feldspar pores, and kaolinite aggregates are closely associated thin platelets (Figs. 5I and 6B). Early diagenetic chlorite rims can be identified in some samples. No authigenic illite was identified in the sandstones taken from a depth of 2000 m–4000 m.

#### 4.3.2. Carbonate diagenesis

Three types of carbonate cements including early-diagenetic calcite, early-diagenetic dolomite and late-diagenetic Fe-containing calcite were identified in sandstones (Fig. 7). The early-diagenetic calcite occurs as a microsparry or sparry, interlocking mosaic of crystals, filling primary pores and replacing some detrital grains. In these early-diagenetic calcite cemented sandstones, the cement occupies almost all primary pores and can account for 25%–30% of the total volume in sandstone where leaching of calcite did not occur (Fig. 7A). Early-diagenetic calcite appears to be etched in many samples, which can be interpreted to indicate extensive dissolution of these cements in some sandstones (Fig. 7C–H). In general, early-diagenetic calcite cemented sandstones or sandstones with extensive dissolution of early-diagenetic calcite cements are usually supported by detrital grains with just point contacts, or have a floating texture (Fig. 7A, G), indicating that little compaction have taken place when cementation occurred. Dolomite cement and late-diagenetic Fe-containing calcite were identified in a few samples with depth greater than 3000 m. Late-diagenetic Fe-containing calcite can be identified to fill secondary pores formed by feldspar dissolution (Fig. 7B), indicating that it is formed after feldspar leaching reactions. In addition to the dissolution of early-diagenetic calcite cements, dissolution of detrital carbonate grains can also be identified in many thin sections (Fig. 7I).

#### 4.4. Fluid inclusions

Secondary fluid inclusions in healed microfractures in quartz grains are abundant (Fig. 8B), while primary fluid inclusions in

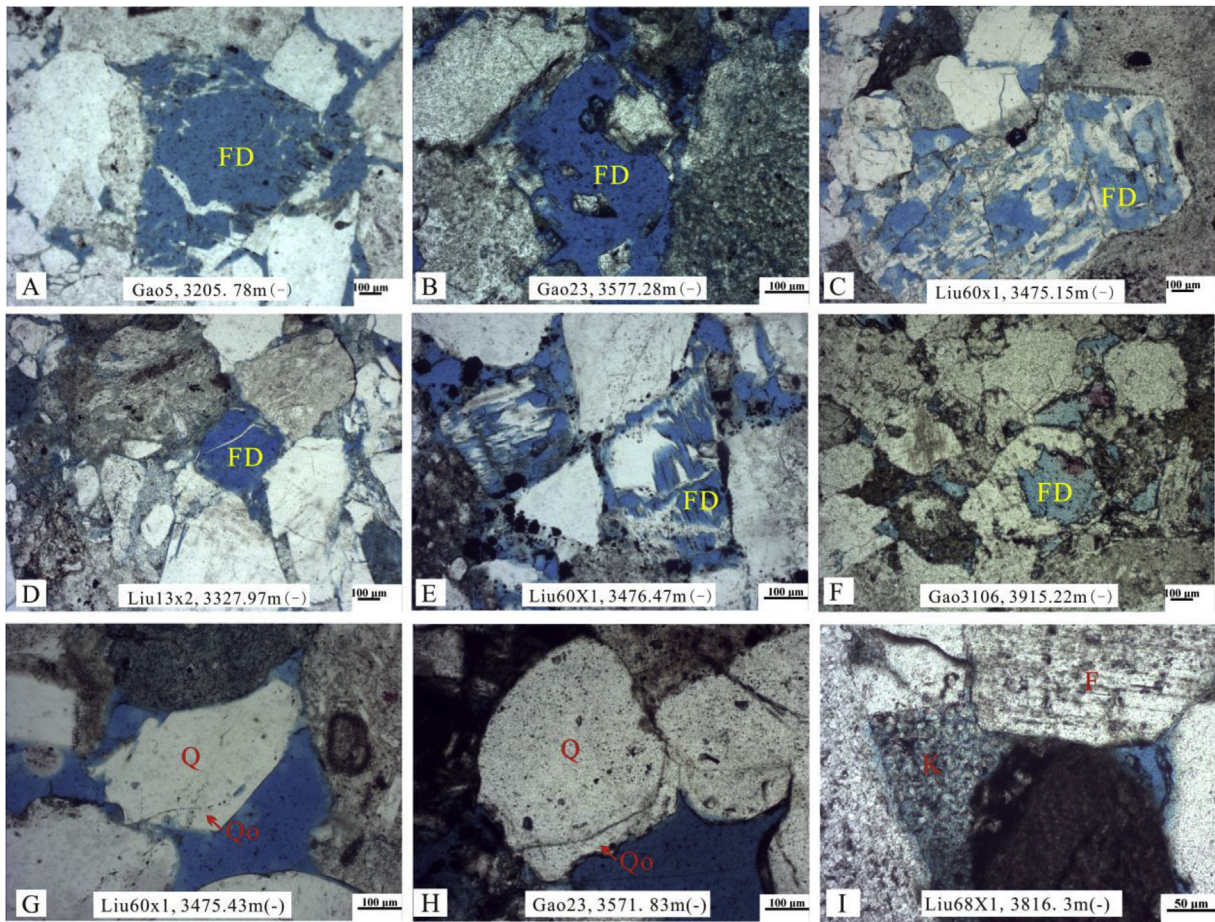


**Fig. 5.** Photomicrographs of leached feldspar and associated secondary minerals in sandstone thin sections. Blueness in the thin section represents pore space. A–F: extensive leached feldspars with little precipitation of secondary minerals in the secondary pores in most of the thin sections. Secondary pores after feldspar grains preserve original outlines of former grain. G–H: quartz overgrowths in a few thin sections. I: Kaolinite in some primary pores, blue epoxy resin can be identified in the kaolinite aggregates, indicating the presence of micropores among these plates. Note: F-detrital feldspar grain, FD-secondary pores formed by feldspar dissolution, Q-detrital quartz grain, Qo-quartz overgrowths, K-authigenic kaolinite. (For interpretation of the references to colour in this figure legend, the reader is referred to the web version of this article.)

quartz overgrowths are not common (Fig. 8A). The size of the AFLs in healed microfractures ranges from 2  $\mu\text{m}$  to 11  $\mu\text{m}$ , and the size of AFLs in quartz overgrowths ranges mainly from 2  $\mu\text{m}$  to 8  $\mu\text{m}$ . The test data show the  $T_h$  of AFLs in healed microfractures is mostly in the range of 95  $^{\circ}\text{C}$ –125  $^{\circ}\text{C}$ . Because quartz overgrowths are scarce in these reservoir samples, only a few AFLs in quartz overgrowths were analyzed. The  $T_h$  of these AFLs ranges mainly from 95  $^{\circ}\text{C}$  to 115  $^{\circ}\text{C}$  (Table 2) (see Fig. 9).

#### 4.5. Oxygen isotope compositions

##### 4.5.1. Oxygen isotope compositions of quartz

With the completion of ion microprobe analysis, all analyzed pits were examined using optical and CL microscopes to determine the exact nature of the quartz (Fig. 10). The  $\delta^{18}\text{O}$  values of the four analyzed rocks are shown in histogram form in Fig. 11. These  $\delta^{18}\text{O}_{(\text{SMOW})}$  values within quartz grains range mainly from 8‰ to 13‰, and  $\delta^{18}\text{O}_{(\text{SMOW})}$  values of pure quartz overgrowths are mostly in the range of 17‰–20‰.

##### 4.5.2. Oxygen isotope compositions of carbonate mineral

The isotopic composition of carbonate cements was measured in 10 sandstone samples, and types and contents of carbonate cements in these samples were counted within the thin sections (Table 3). Most early-diagenetic calcite has a relatively wide range

of  $-7\text{‰}$  to  $-13\text{‰}$  for  $\delta^{18}\text{O}_{(\text{PDB})}$  values and  $-2\text{‰}$  to  $-7\text{‰}$  for  $\delta^{13}\text{C}$ . Late-diagenetic Fe-containing calcite has a range of  $-15\text{‰}$  to  $-19\text{‰}$  for  $\delta^{18}\text{O}_{(\text{PDB})}$  and  $-2\text{‰}$  to  $-7\text{‰}$  for  $\delta^{13}\text{C}$ .

#### 4.6. Pore water chemistry

Data of the 242 pore-water samples from the Shahejie sandstone reservoirs in the GL area are presented in Fig. 12 and Fig. 13. More than 90% of the pore waters are characterized by  $\text{NaHCO}_3$  water, with the remaining 10% being composed mainly of  $\text{CaCl}_2$  water,  $\text{MgCl}_2$  water or  $\text{Na}_2\text{SO}_4$  water (Fig. 12). Generally, pore water salinity is very low in these samples, ranging from 0.79 g/L to 6.77 g/L, and shows no obvious vertical variation from the Ng Formation to the Es3 sub-member (Fig. 13). Also, ion concentrations of different solutes are generally low and have no sharp vertical variation.

## 5. Discussion

### 5.1. Diagenetic evolution history

#### 5.1.1. Diagenetic sequences

With constraints of the detailed petrography, the isotopic compositions of the authigenic minerals and the homogenization temperature ( $T_h$ ) of the aqueous fluid inclusions, general diagenetic

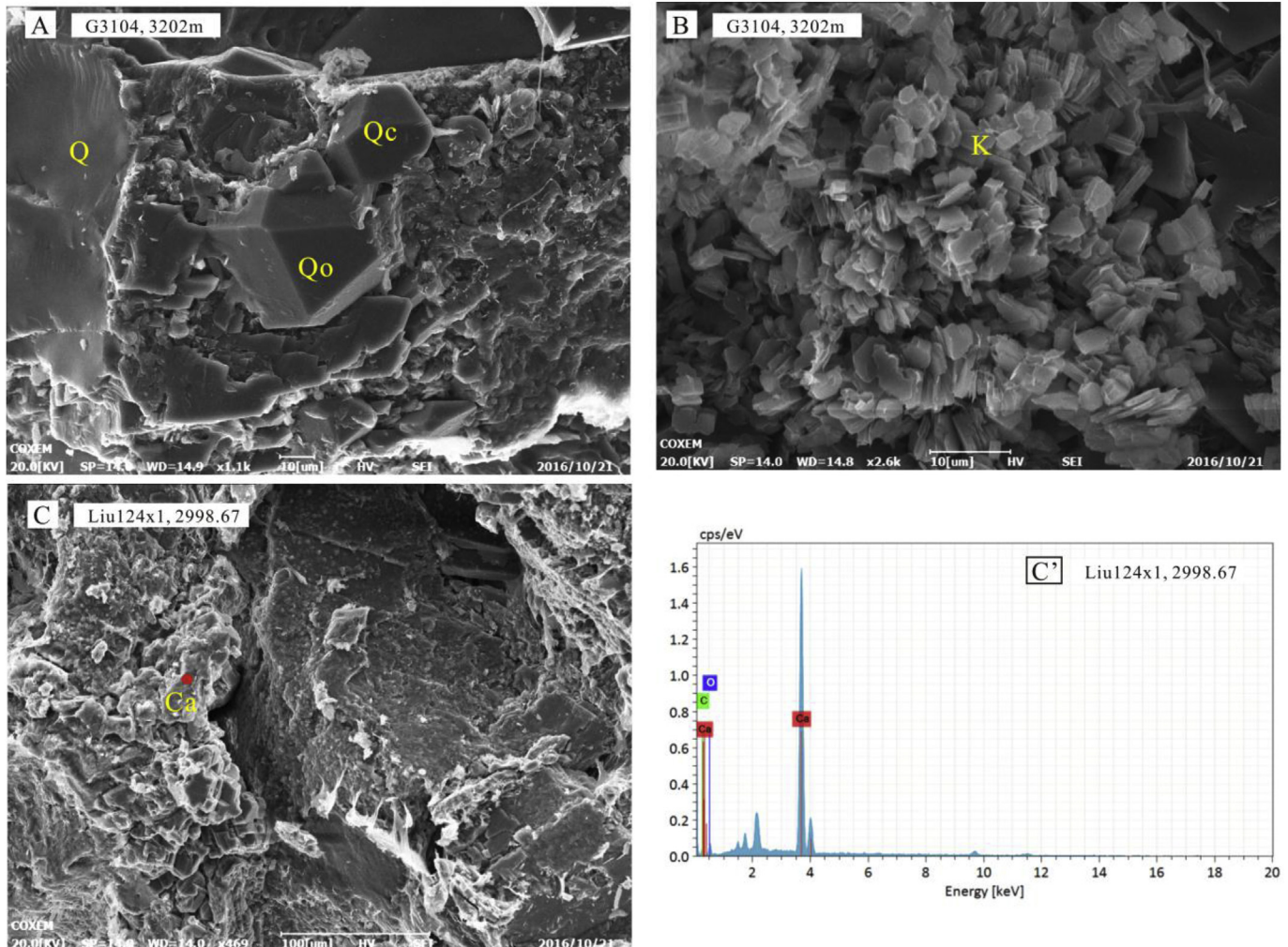


**Fig. 6.** SEM images of quartz cements, kaolinite, and leached calcite cements in the Shahejie sandstones in the Gaoliu area. A: quartz overgrowths (Qo) and quartz crystals (Qc); B: authigenic kaolinite (K); C: remnant calcite cements after leaching reaction (Ca), red solid circle represents an EDS analyzing spot. C': EDS tested composition of the calcite in figure C. (For interpretation of the references to colour in this figure legend, the reader is referred to the web version of this article.)

sequences of the Shahejie sandstones in the Gaoliu area can be summarized as in Fig. 14. The composite diagenetic sequences include compaction and carbonate cementation in the eodiagenetic stage during the initial burial, subsequent dissolution of early-diagenetic calcite cement and feldspars and precipitation of kaolinite during the uplift and the initial reburial stage, continuing dissolution of feldspars and precipitation of some authigenic quartz, kaolinite and some late carbonate cements in the meso-diagenetic stage during the late period of the reburial stage. Approximate temperatures and times for the occurrence of different diagenetic reactions are discussed below.

### 5.1.2. Temperature and time for feldspar diagenesis

The timing of feldspar dissolution in sandstones could be early syn-sedimentary, associated with unconformities, or taking place during late burial (Bjørlykke and Jahren, 2012; Molenaar et al., 2015). Secondary pores formed from detrital feldspar dissolution do not preserve the geochemical identity of which caused the dissolution. Several lines can be used to investigate the relative timing of feldspar dissolution. First, feldspar dissolution occurred mainly in porous sandstones (Fig. 5), whereas the low porosity sandstones with massive early-calcite cements generally contain limited feldspar pores (Table 1; Fig. 7A), suggesting that extensive

feldspar dissolution occurred mainly after early-diagenetic calcite cementation (Yuan et al., 2015c). Second, the timing of the detrital feldspar dissolution and new growth of minerals can be assessed relative to compaction features (Molenaar et al., 2015). Oversized pores from early shallow grain dissolution that developed before the maximum packing density and a collapsed but stable grain framework was reached, would have been destroyed by framework collapse in deeply-buried sandstones (Wilkinson et al., 2001), and early formed authigenic clay fabrics would also have been deformed by later compaction (Molenaar et al., 2015). In this study, however, the secondary pores after feldspar grain dissolution have preserved the original outlines of the former grains (Fig. 5A–D), and authigenic kaolinite was not affected by compaction, retaining its pseudo hexagonal or vermicular shapes (Figs. 5I and 6B). The early syn-sedimentary leaching reactions were not completely excluded, but petrography textures (Figs. 5–7) suggest that the feldspar dissolution probably occurred mainly after the eodiagenetic stage, when compaction and early-diagenetic cementation were dominant. Third, results of laboratory feldspar dissolution experiments using fluids far from equilibrium show that the rate constant for feldspar dissolution increases by a factor of about 10,000 as temperature increases from 20 °C to 120 °C (Thyne, 2001). Occurring in a relative open sandstone geochemical system (as discussed in

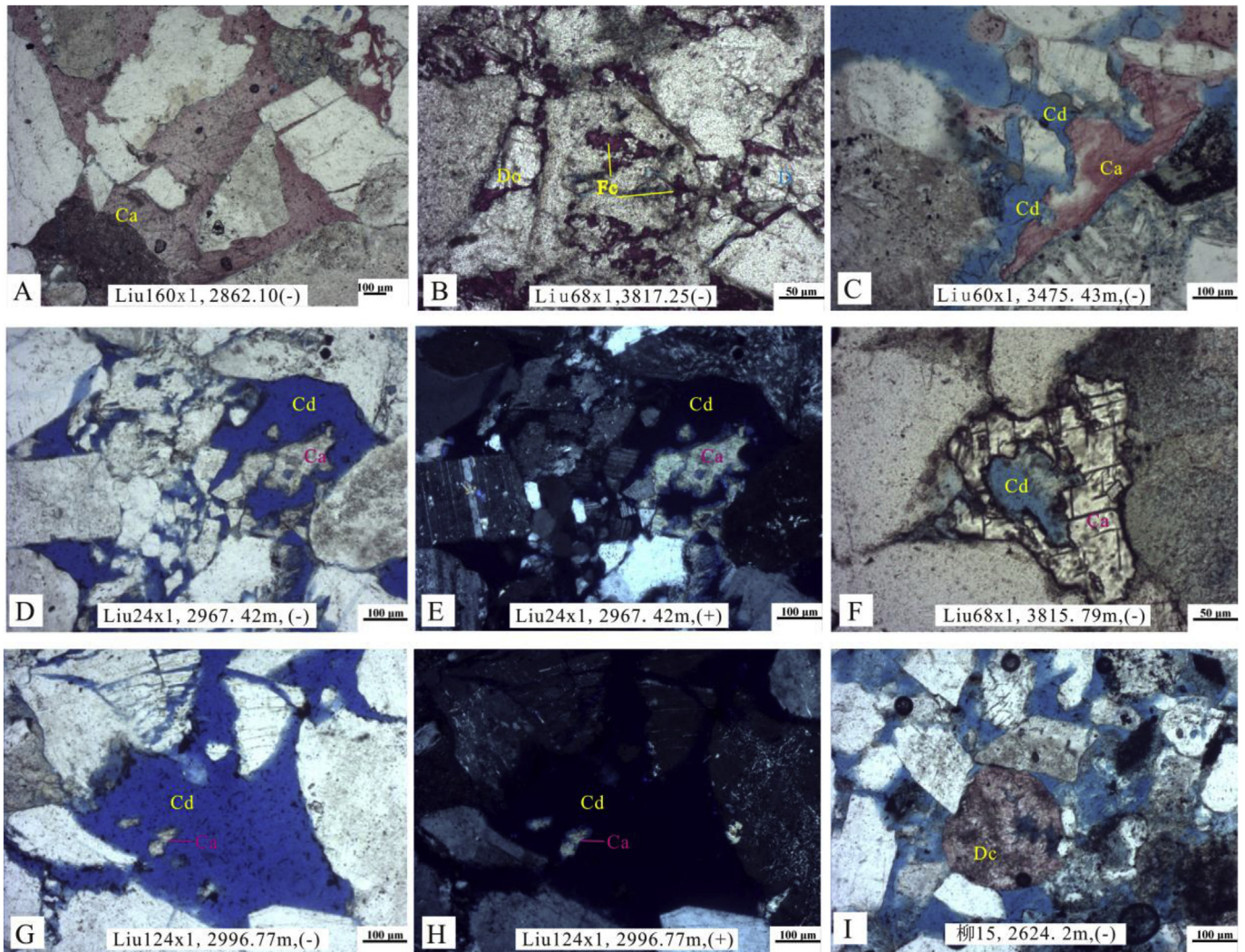


**Fig. 7.** Photomicrographs of carbonate cements and leaching texture of early-diagenetic calcite in sandstone thin sections. Bluesness represents pore space. A—low porosity sandstones with large volume of carbonate cements; B—late calcite cements in feldspar pores. C—H: extensive dissolution of early carbonate cements; oversized pores (Fig. 7G) and remnant calcite cements can be identified. I: dissolution of detrital calcite grain. D–E and G–H are the same views presented using plane-polarized light and cross-polarized light. Ca: early calcite cement, Fc: late calcite cement, Do: dolomite, Cd: secondary pores formed by dissolution of early-diagenetic calcite cement, Dc: detrital calcite grain. (For interpretation of the references to colour in this figure legend, the reader is referred to the web version of this article.)

Section 4.2) with weak precipitation of secondary minerals, the dissolution rate of feldspars depends largely on temperature and saturation state of pore water (Zhu et al., 2004, 2010). At present, pore water with low concentration of  $K^+$  (Fig. 13) is still undersaturated with respect to the remaining feldspar compositions in

the sandstones (Bjørlykke, 1998), and thus, the leaching processes should still be active, though hydrocarbon in the reservoirs may slow down such reactions to some extent. Fourth, the AFIs tested in this study were located within the quartz overgrowths, and resetting and leakage of these primary AFIs as a result of subsequent

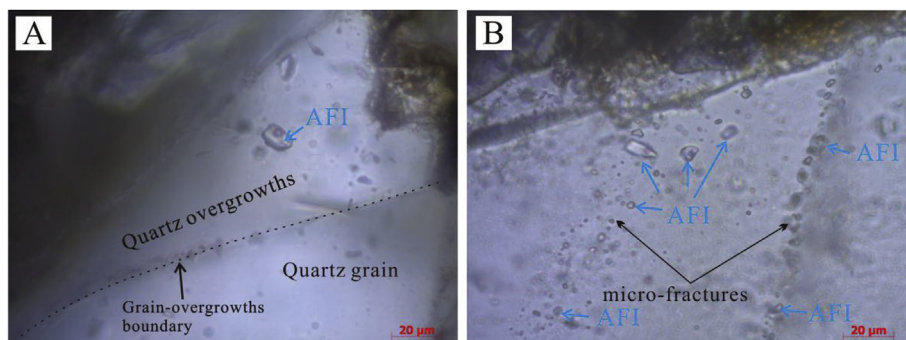


**Fig. 8.** Photomicrographs of aqueous fluid inclusions (AFI) under transmitted light observed at room temperature in the Shahejie sandstones in the Gaoliu area. (A) AFIs in quartz overgrowth; (B) AFIs in healed microfractures in quartz grains.

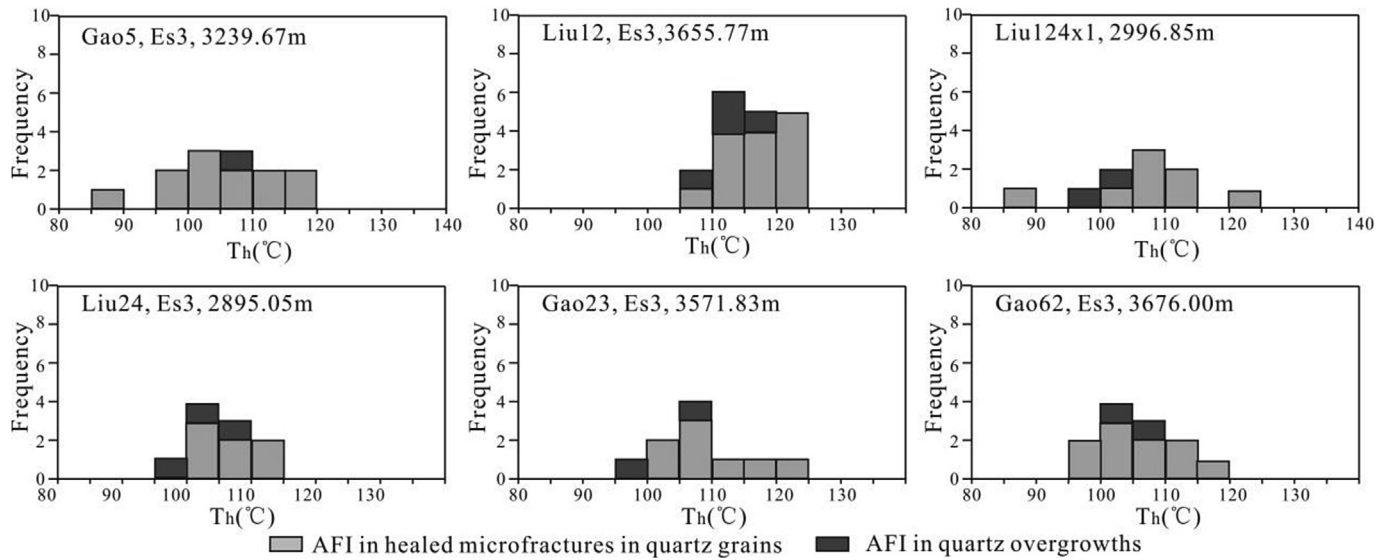


Fig. 9.  $T_h$  distribution of aqueous fluid inclusions in healed microfractures and in quartz overgrowths in the Shahejie sandstones in the Gaoliu area.

Table 2

Microthermometric data of aqueous fluid inclusions in the Shahejie sandstones in the Gaoliu area.  $T_h$ : homogenization temperature.

Well	Depth, m	Strata	Distance to unconformity beneath the Ng Formation, m	Aqueous inclusions in healed microfractures in quartz grains		Aqueous inclusions in quartz overgrowths	
				Size, $\mu\text{m}$	$T_h$ , $^{\circ}\text{C}$ (Number)	Size, $\mu\text{m}$	$T_h$ , $^{\circ}\text{C}$ (Number)
Gao5	3239.67	Es <sub>3</sub>	1213.67	2–8	90–120 (12)	5	107 (1)
Liu12	3655.77	Es <sub>5</sub>	1640.27	2–11	107–127 (14)	3–8	105–117 (4)
Liu124x1	2996.85	Es <sub>3</sub>	825.35	2–6	88–123 (8)	3–6	95–105 (2)
Liu24	2895.05	Es <sub>4</sub>	723.05	3–8	100–109 (5)	6	98–110 (3)
Gao23	3571.83	Es <sub>3</sub>	1606.83	3–10	102–125 (8)	2–6	103–114 (2)
Gao62	3676.00	Es <sub>3</sub>	1169	2–9	97–123 (10)	3–6	95–109 (2)

burial is unlikely (Girard et al., 2001), which is also verified by the spherical or elliptical shape of these AFIs (Fig. 8A). Thus, the  $T_h$  data (95–115  $^{\circ}\text{C}$ ) of the tested fluid inclusions (Table 2) represent the starting precipitation temperature of the quartz overgrowths. The  $T_h$  data of AFIs in these quartz overgrowths was plotted on the burial and thermal history chart, which suggested that these quartz overgrowths probably were formed at burial depth greater than 2500 m, from approximately 12 Ma years ago to now (Fig. 2A). This also indicates that feldspar dissolution may still be occurring at present, and only such late stage feldspar dissolution was accompanied by quartz cementation.

### 5.1.3. Temperature and time for carbonate diagenesis

$\delta^{18}\text{O}_{(\text{SMOW})}$  values of current river waters in the Beijing area and pore waters with low salinity (<2 g/L) from shallow sediments deposited in fluvial setting in the Bohai Bay Basin range from  $-11\text{‰}$  to  $-8\text{‰}$  (Song et al., 2006; Sun et al., 1982). High salinity lake water in the Dongying Sag during the deposition period of the Shahejie Es4 member was suggested to have an average  $\delta^{18}\text{O}_{(\text{SMOW})}$  value of  $-4.8\text{‰}$  (Yuan et al., 2015c). With positive relationships between  $\delta^{18}\text{O}$  values and pore water salinity (Clayton et al., 1966), the saline lake water in the Gaoliu area during the deposition period of the Shahejie Formation probably had  $\delta^{18}\text{O}_{(\text{SMOW})}$  values ranging from  $-9\text{‰}$  to  $-5\text{‰}$ .  $\delta^{18}\text{O}_{(\text{SMOW})}$  values of the early-diagenetic calcites ranges mainly from  $14\text{‰}$  to  $16.5\text{‰}$  (Table 3). Using oxygen isotope fractionation factor for calcite-water from Friedman and O'Neil (1977), the early-diagenetic calcite cements were calculated to be precipitated at 50  $^{\circ}\text{C}$  - 80  $^{\circ}\text{C}$  (Fig. 15), during the initial

burial stage. This was also verified by the petrographic texture of point contacts of detrital grains or floating textures in the sandstones with large amounts of the early-diagenetic calcite cements (Fig. 7A), or oversized pores formed by dissolution of the early-diagenetic calcite cements (Fig. 7G).

During the initial burial stage, precipitation of calcite likely dominated chemical reactions as connate alkaline pore water played an important role in the eodiagenetic stage. Though organic acids and  $\text{CO}_2$  were likely generated in the Es<sub>3</sub> - Es<sub>5</sub> sub-members when temperature of these strata reached 70–80  $^{\circ}\text{C}$  at the end of the initial burial stage, it was not likely that extensive dissolution of calcite cements occurred because of the limited pore water volume (Yuan et al., 2015a). During the uplift and initial reburial stages, the great uplift that the Gaoliu area experienced led to the development of a topographically hydraulic head. With the development of faults connecting the earth's surface and the sandstones in the Shahejie Formation, the uplift likely promoted the incursion of meteoric freshwater into these sandstones (as discussed in Section 4.2) (Bjørlykke, 1993). Thus, the most likely time for calcite dissolution would have been during the uplift and initial reburial stages.

With constraints of  $T_h$  data (95–115  $^{\circ}\text{C}$ ) of AFIs, in situ  $\delta^{18}\text{O}_{(\text{SMOW})}$  values ( $+17\text{‰}$ ~ $+20\text{‰}$ ) within the quartz overgrowths and an quartz-water oxygen isotope fractionation equation (Méheut et al., 2007), oxygen isotopic compositions of paleo-fluids ( $\delta^{18}\text{O}_{(\text{SMOW})}$ ) in which the quartz overgrowths were formed are calculated to be between  $-7\text{‰}$  and  $-2\text{‰}$  (Fig. 16). It is reasonable to suggest that the water formed the late-diagenetic calcite have a similar  $\delta^{18}\text{O}_{(\text{SMOW})}$  of  $-7\text{‰}$  to  $-2\text{‰}$  as late-stage calcite was

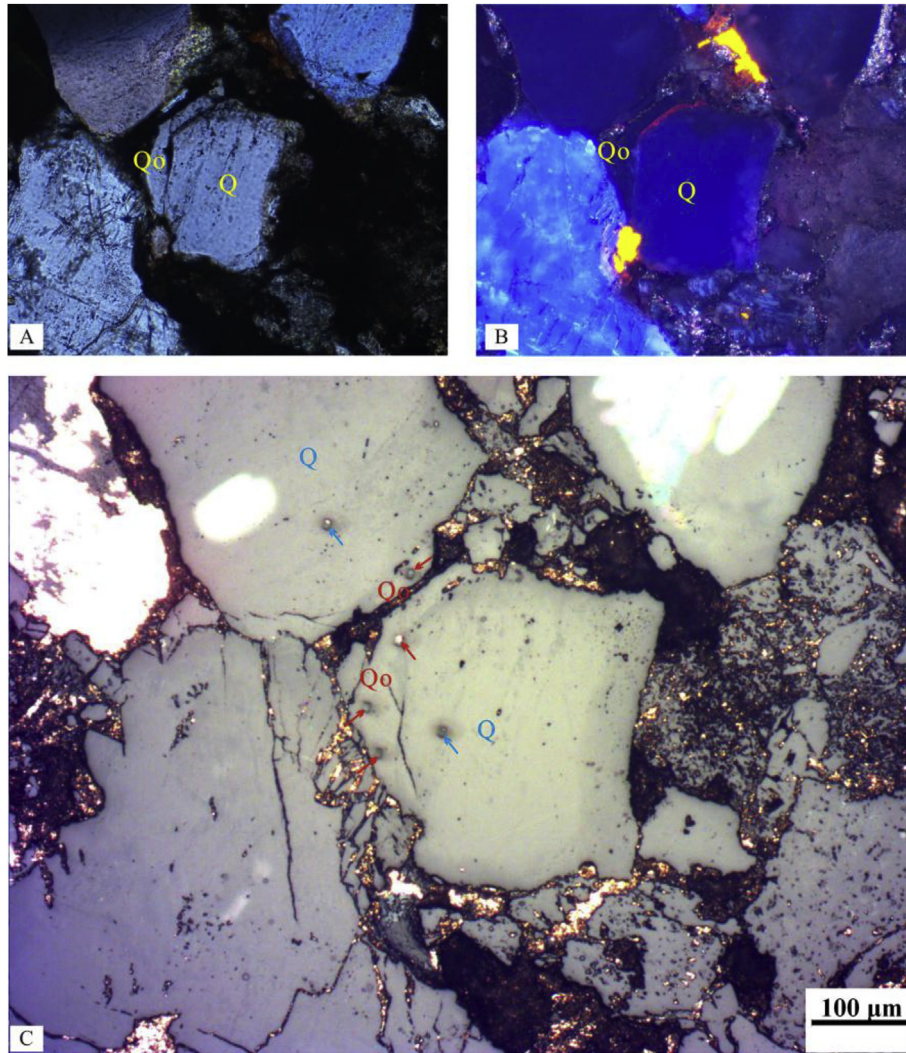


**Fig. 10.** Petrography of quartz overgrowths identified with optical and CL microscopy. A, B: Plane-polarized light (PPL) and cathodoluminescence (CL) views showing quartz overgrowths in sandstones at 2996.85 m in well Liu-124X1, C: reflected views showing ion microprobe pits generated from SIMS analysis of oxygen isotopes. Q: detrital quartz grain; Qo: authigenic quartz overgrowth.

precipitated no earlier than feldspar dissolution. Using the oxygen isotope fractionation factor for calcite-water from Friedman and O'Neil (1977), the late-diagenetic calcite cements were calculated

to be precipitated at 80°C–120 °C (Fig. 15) (Yuan, 2015), which is consistent with petrography texture relationships (Fig. 7B).

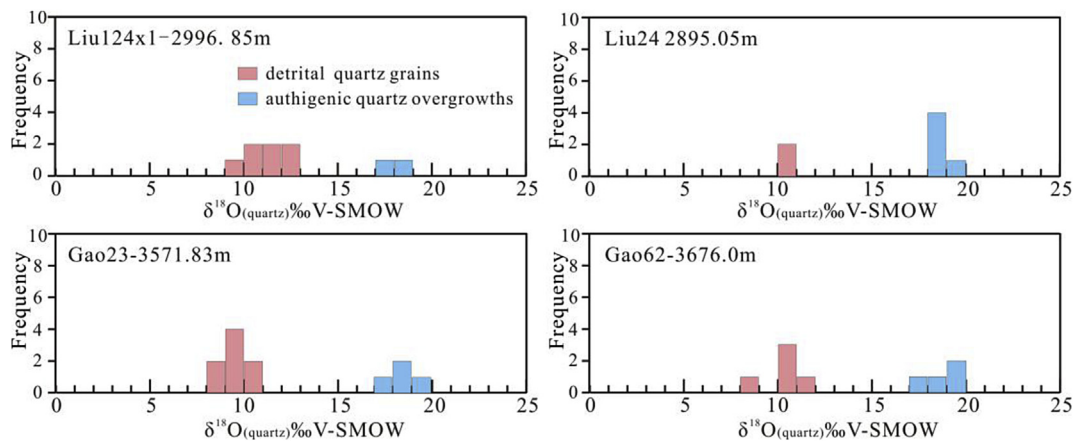


**Fig. 11.** Histograms showing the distribution of  $\delta^{18}\text{O}(\text{quartz})\text{‰ V-SMOW}$  values of detrital quartz grains and authigenic quartz overgrowths in four samples.

**Table 3**  
Mineralogical and isotopic composition of carbonate cements in the Shahejie sandstones in the Gaoliu area, Nanpu Sag. Ca: early diagenetic calcite; Fc: late-diagenetic Fe-containing calcite.

Well	Depth (m)	Carbonate cements	Carbonate cement content,	$\delta^{13}\text{C}_{\text{-PDB}}$ (‰)	$\delta^{18}\text{O}_{\text{-PDB}}$ (‰)	$\delta^{18}\text{O}_{\text{-SMOW}}$ (‰)
Gao66	3884.25	100%Ca	10%	-11.38	-19.55	10.76
Gao81	2913.05	100%Ca	25%	-3.52	-14.32	16.15
Gao3105	3682.51	100%Ca	2%	-6.26	-14.64	15.81
Gao3105	3554.66	90%Fc+10%Ca	6%	-1.85	-17.15	13.23
Liu12	3657.7	90%Fc+10%Ca	5%	-6.73	-15.83	14.59
Liu22	3207.40	100%Fc	1%	-2.76	-14.42	16.05
Liu68x1	3816.5	90%Fc+10%Ca	2%	-6.69	-17.36	13.01
Liu68x1	3794.45	100%Fc	0.5	-0.26	-17.39	12.99
Liu124x1	2819.93	100%Ca	13 (partially dissolved)	-5.62	-15.42	15.01
Liu124x1	2967.42	100%Ca	2 (extensively dissolved)	-4.85	-14.36	16.11

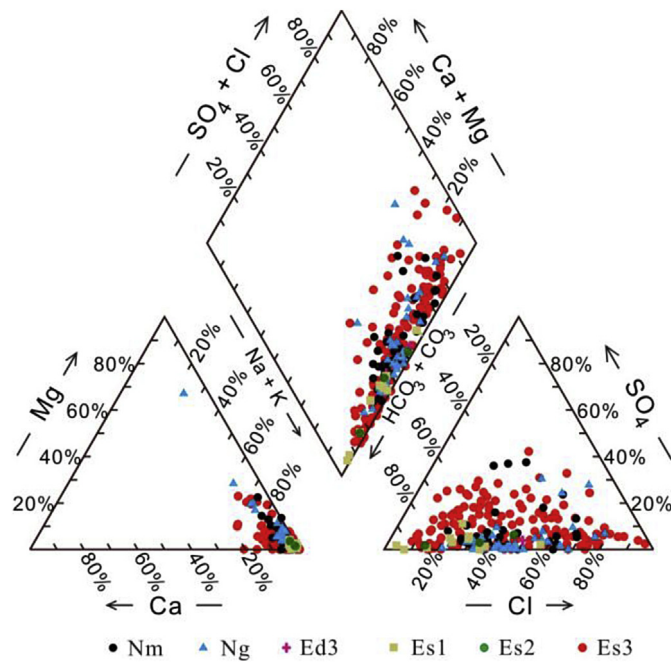


**Fig. 12.** Piper diagram showing major ion composition in pore water from sandstone reservoirs of different formations in the Gaoliu area, Nanpu Sag.

5.2. Open geochemical system and pore water evolution

5.2.1. Mass imbalance and mass transfer in geochemical system

In a closed sandstone geochemical system without large-scale advective flow, feldspars are generally leached to form secondary

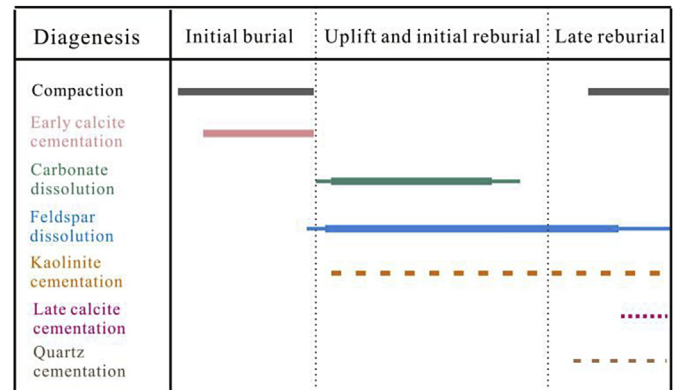


**Fig. 14.** General diagenetic sequences of the Shahejie sandstones in the Gaoliu area, Nanpu Sag.

pores and almost equal volumes of in situ secondary minerals including clays (kaolinite or illite) and quartz cements with respect to the feldspar-hosted secondary pores (Giles and De Boer, 1990; Higgs et al., 2007; Molenaar et al., 2015). In the sandstones of the present study, the amount of feldspar-hosted secondary pores obtained from the only 2D thin sections reaches as high as 3–5%, whereas the authigenic kaolinite content is generally less than 0.5–1.0% of the total rock and the authigenic quartz content is generally less than 0.1% (Table 1; Fig. 17). The great differences between the expected volume of secondary minerals and actual volume of such minerals (Fig. 17) demonstrate that only a small portion of  $\text{Al}^{3+}$ ,  $\text{SiO}_2(\text{aq})$ , and  $\text{K}^+$  released by feldspar dissolution was preserved in the sandstone geochemical system through secondary mineral precipitation. Early-diagenetic calcite cements

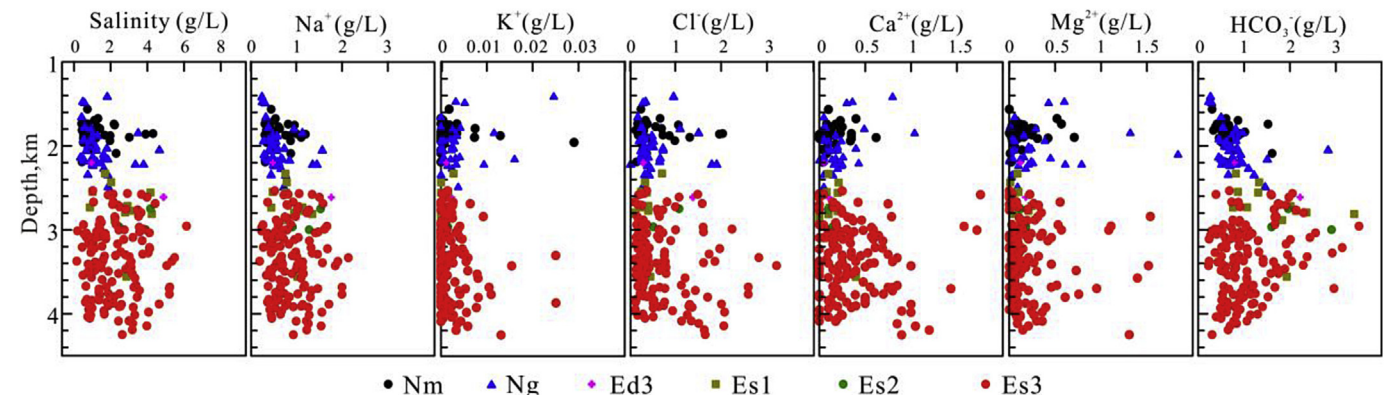


**Fig. 13.** Salinity and concentration of different ions in pore waters from different formations in the Gaoliu (GL) area, Nanpu Sag (After Yuan et al., 2015b).

were identified to be leached extensively (Fig. 7), but few late-diagenetic calcite cements were precipitated to preserve leached  $\text{Ca}^{2+}$  solutes in most sandstone samples. Without mineral precipitation, the dissolution of 1% volume of feldspar and calcite would produce high concentrations of  $\text{K}^+$  (>2 g/L) and  $\text{Ca}^{2+}$  (>10 g/L) in interbedded sandstone–mudstone systems with mudstone/sandstone ratio less than 5:1 in the Shahejie Formation in the Gaoliu area. Because of this, the low water salinity and low concentration of these ions in the pore waters (Fig. 13) deny the preservation of these solutes in the pore waters of the sandstones. All in all, the available petrography and pore water data suggest that these solutes were indeed removed from the sandstone system, indicating an open sandstone geochemical system for relevant water–rock interactions.

Diffusion, convection, and advection are the three ways to transport solutes in porous rocks (Bjørlykke and Jahren, 2012; Thyne, 2001; Wood and Hewett, 1982). Three models can be considered for the diagenetic mineral assemblage of large amounts of leached feldspars with few associated secondary minerals: (1) Solute released from sandstones were transported into interbedded mudstones by diffusion; (2) Solute were redistributed in individual sandstone beds by convection; (3) Solute were removed from sandstones by advective flow.

Model 1: Diffusion dominated mass transfer in interbedded sandstone–mudstone systems. Numerical simulations on mass transfer between adjacent sandstones and mudstones conducted by Thyne (2001) demonstrate that ① extensive transfer of  $\text{Al}^{3+}$  and  $\text{SiO}_2(\text{aq})$  from sandstones to mudstones is not likely to occur as the transition reaction from smectite to illite and dissolution of feldspars in mudstones also releases  $\text{Al}^{3+}$  and  $\text{SiO}_2(\text{aq})$ . And the  $\text{Al}^{3+}$  and  $\text{SiO}_2(\text{aq})$  released by feldspar dissolution in sandstones would be consumed through precipitation of secondary minerals in the sandstones; ② more feldspars will be leached in marginal sandstones close to the sandstone–mudstone interface if the smectite–illite transition reactions in interbedded mudstones consumes the potassium transferred from sandstones by diffusion (Thyne, 2001). However, in the Shahejie sandstones of this study, feldspars in the

marginal sandstones near the sandstone/mudstone interface were not identified to be leached more extensively than those in the central sandstones, indicating that diffusion on its own cannot interpret the diagenetic petrography textures in these sandstones.

Model 2: Supposing thermal convection occurred and dominated the pore water flow in an individual sandstone bed, pore water circulation in the sandstone bed would likely redistribute solutes released from leached feldspar and calcite minerals, leading to dissolution in specific zones and precipitation in others within the sandstone bed (Wood and Hewett, 1982). However, no such diagenetic pattern was identified in the sandstone bed samples, meaning no occurrence of large scale thermal convection.

Model 3: As diffusion and convection could not produce the diagenetic phenomena in the sandstones, advection should be the most likely of the three candidates. Supposing large amounts of advective flows were injected into the sandstone beds in geologic time, these advective flows could remove solutes from the dissolution zones and sandstone beds. The low water salinity, low concentration of different ions, the low salinity gradient (Fig. 13), and negative hydrogen isotope compositions of present pore water (Zhang et al., 2008) suggest that meteoric freshwater must be a vital source of such present water. Still, we need to investigate when and how the incursion of the freshwater into the Shahejie Formation sandstones occurred.

#### 5.2.2. Ancient “deep” incursion of meteoric freshwater

Evidence for pressure dissolution of detrital quartz is rather weak in the studied sandstones (Figs. 5–7), and so it is safe to assume that the feldspar dissolution most likely provided silica for the quartz cements. The pore water responsible for forming the quartz overgrowths was characterized by relatively high temperature (95–115 °C) and negative  $\delta^{18}\text{O}_{(\text{SMOW})}$  (–7‰ to –2‰) composition (Fig. 16). This negative  $\delta^{18}\text{O}_{(\text{SMOW})}$  data suggests that the quartz cementation and simultaneous late stage feldspar dissolution occurred in meteoric derived pore water that had been previously modified by water–rock interactions during diagenesis (Aplin and Warren, 1994; Harwood et al., 2013). Three scenarios can

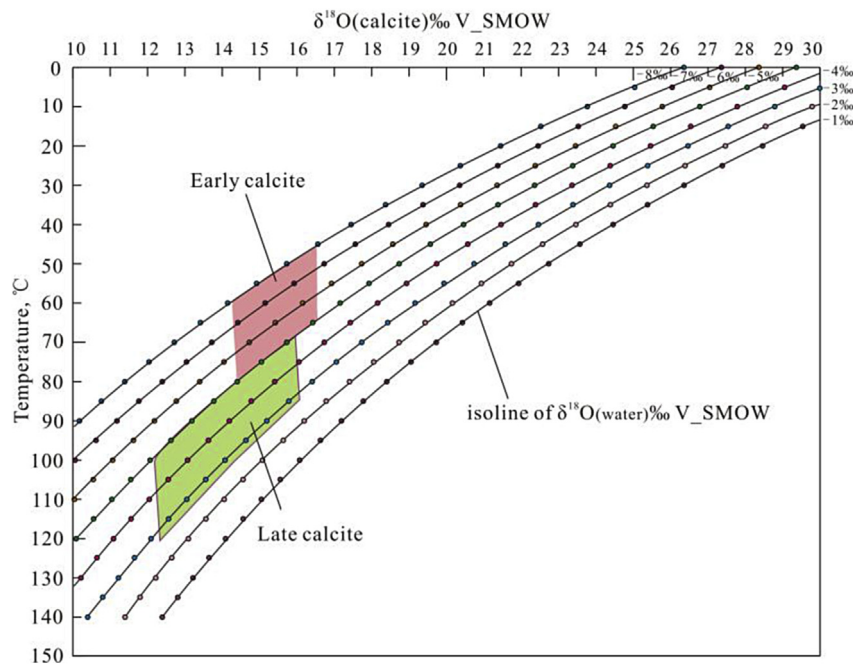


Fig. 15. Cross plot of calcite  $\delta^{18}\text{O}_{(\text{SMOW})}$  values of the carbonate cements in the Shahejie sandstones in the Gaoliu area in equilibrium with water  $\delta^{18}\text{O}_{(\text{SMOW})}$  values (–8‰, –7‰, –6‰, –5‰, –4‰, –3‰, –2‰, –1‰) as a function of temperature (Friedman and O’Neil, 1977).

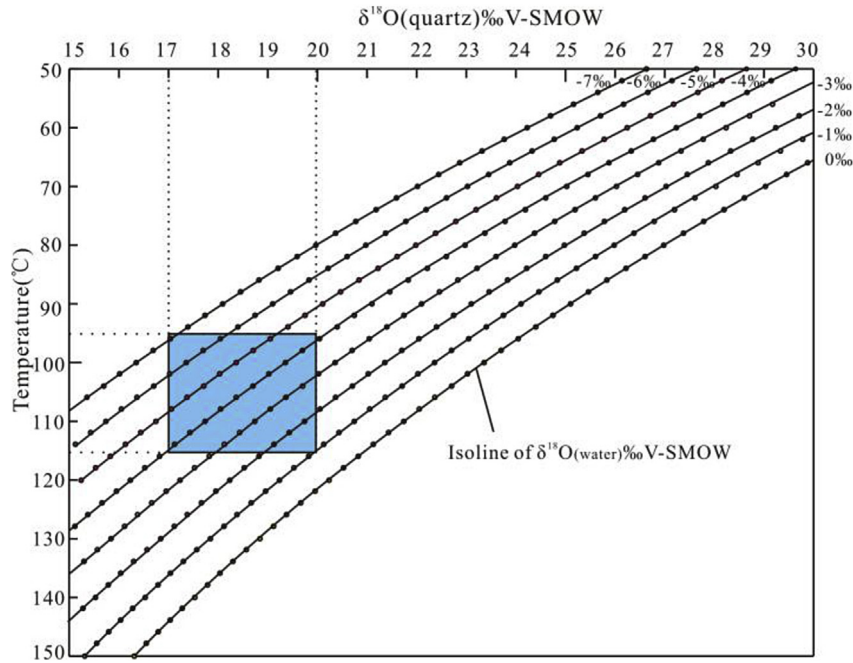


Fig. 16. Cross plot of quartz  $\delta^{18}\text{O}_{(\text{SMOW})}$  values in equilibrium with water  $\delta^{18}\text{O}_{(\text{SMOW})}$  values ( $-7\text{‰}$ ,  $-6\text{‰}$ ,  $-5\text{‰}$ ,  $-4\text{‰}$ ,  $-3\text{‰}$ ,  $-2\text{‰}$ ,  $-1\text{‰}$ ,  $0\text{‰}$ ,  $+1\text{‰}$ ,  $+2\text{‰}$ ,  $+3\text{‰}$ ) as a function of temperature (Méheut et al., 2007).

be considered for the genesis of such diagenetic modified pore water (Fig. 18): (1) Connate lake water with a negative  $\delta^{18}\text{O}_{(\text{SMOW})}$  value of  $-9\text{‰}$  to  $-5\text{‰}$  was modified gradually to between  $-7\text{‰}$  and  $-2\text{‰}$ , without incursion of meteoric freshwater during the burial process. (2) Connate lake water with a negative  $\delta^{18}\text{O}_{(\text{SMOW})}$  value was modified to pore water with  $\delta^{18}\text{O}_{(\text{SMOW})}$  values higher

than  $-2\text{‰}$  gradually, then deep incursion of meteoric freshwater during the late reburial stage decreased the  $\delta^{18}\text{O}_{(\text{SMOW})}$  value to between  $-7\text{‰}$  and  $-2\text{‰}$ . (3) Meteoric freshwater flushed into the Shahejie sandstones during the uplift and subsequent initial reburial stages (approximately 26–15 Ma) and decreased the  $\delta^{18}\text{O}_{(\text{SMOW})}$  value significantly; the fresh pore water was modified by subsequent diagenesis and hydrocarbon emplacement during the late burial stage, and the  $\delta^{18}\text{O}_{(\text{SMOW})}$  value of the pore water was elevated significantly, particularly during the hydrocarbon charging period.

Scenario 1, without incursion of meteoric freshwater, the  $\delta^{18}\text{O}_{(\text{SMOW})}$  value of pore water would be evaluated gradually by chemical diagenesis (Fayek et al., 2001), similar to the  $\delta^{18}\text{O}_{(\text{SMOW})}$

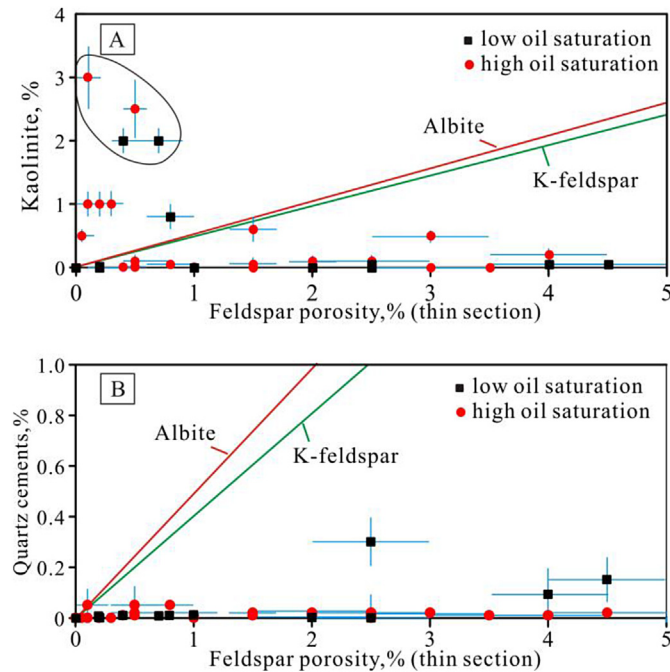


Fig. 17. Plots of the amount of feldspar porosity versus secondary minerals in the thin sections, the few data in the black circle represent a few samples with abundant kaolinite, all from one well. The red and green solid lines represent the expected amount of secondary minerals formed accompanying dissolution of albite or K-feldspar in closed geochemical system. (For interpretation of the references to colour in this figure legend, the reader is referred to the web version of this article.)

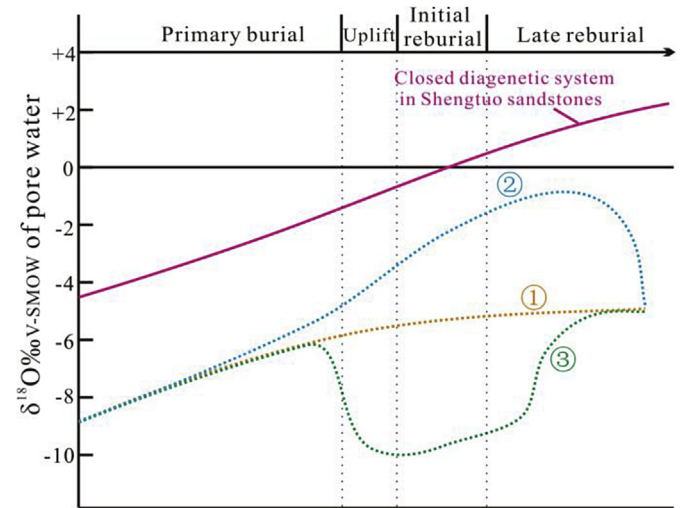
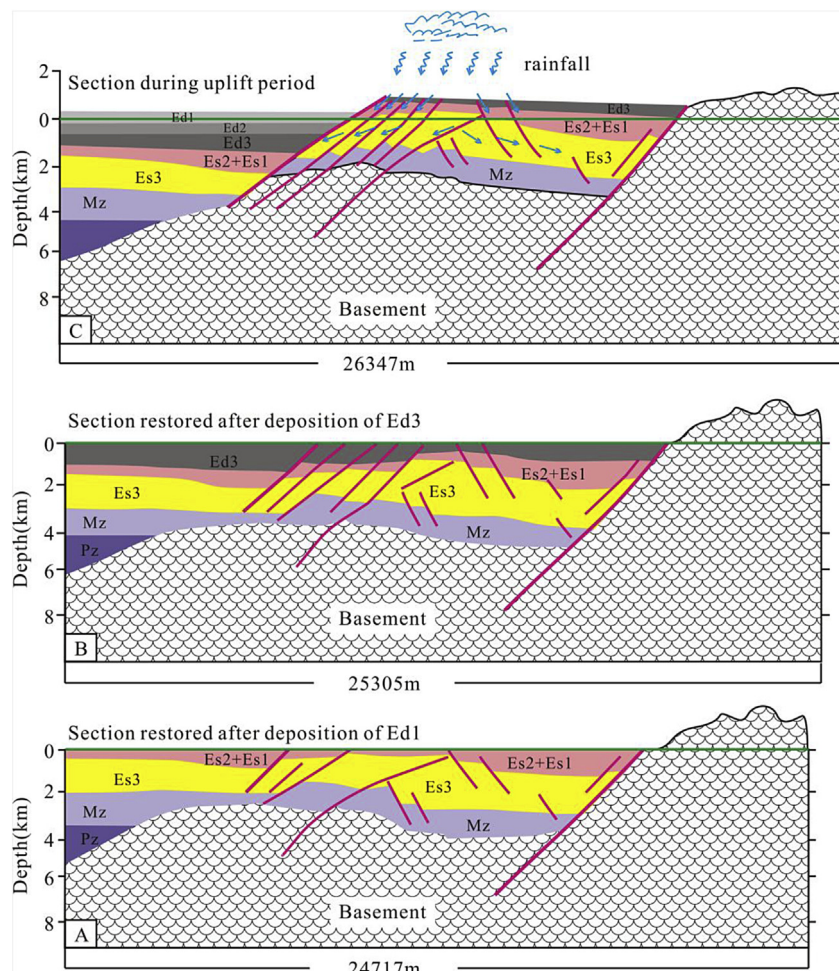


Fig. 18. Possible evolution models of oxygen isotopic compositions of pore water in the open Shahejie sandstones in the Gaoiliu area, Nanpu Sag. Note: ①, ② and ③ represent the three different evolution path of  $\delta^{18}\text{O}$  composition of pore water.

evolutionary path ( $\delta^{18}\text{O}_{(\text{SMOW})}$  value evolved from  $-4.8\text{‰}$  to  $+1.5\text{‰}$   $\sim +4.5\text{‰}$  gradually) of the pore water in a relatively closed turbidite sandstones in the lower Shahejie Formation in the Shengtuo area, Dongying Sag, Bohai Bay Basin (Yuan et al., 2015b). In such a case, however, the limited volumetric pore water would not be able to remove  $\text{Al}^{3+}$  and  $\text{SiO}_2(\text{aq})$  released from feldspar dissolution zones in time, which would lead to in situ precipitation of clays and quartz cements (Giles and De Boer, 1990). This conflicts with the petrographic textures in the Shahejie sandstones in the Gaoliu area (Fig. 5). Furthermore, the low pore water salinity cannot be explained without freshwater input in a geochemical system that has experienced extensive water-rock interactions.

Scenario 2, meteoric water incursion during the late reburial stage (approximately 15–0 Ma) can help to explain the low pore water salinity, the negative  $\delta^{18}\text{O}_{(\text{SMOW})}$  value of paleo-fluid and the carbonate dissolution. However, the diagenetic mineral assemblage of extensively leached feldspars with few associated secondary minerals formed during the uplift and initial reburial stage cannot be explained without freshwater flux. Still, petroleum produced from reservoirs in the Shahejie Formation is generally a light oil with density lower than  $0.85 \text{ g/cm}^3$ , indicating that the hydrocarbons charged during the late Neogene period (approximately 10–5 Ma) have been well preserved, without occurrence of extensive water flushing after hydrocarbon emplacement. Additionally, no water head can be found to account for such deep (2500–4000 m)

freshwater incursion during the late reburial stage. Scenario 3, the Nanpu Sag experienced regional uplift and initial reburial from approximately 26 Ma to 15 Ma. Due to the existence of the Gaoliu fault, the Gaoliu area must have been uplifted more extensively than other structural zones. The eroded strata thickness was estimated to be approximately 600 m in the Gaoliu area by using acoustic travel time logging (AC) calculations (Guo et al., 2013). The uplift height of the Gaoliu area may be much larger than this value, although it is difficult to estimate the specific value. The mountain altitude in the Bohaiwan area can reach up to more than 2000 m, so it is reasonable to assume that the Gaoliu area has been uplifted more than 1000–1500 m above sea level during the uplift stage (Fig. 19), and 600 m strata were eroded during the late Oligocene period. At present, the distance from available sandstone samples to the regional unconformity under the Nm formation (the earth's surface during the uplift period) ranges from 500 m to 1800 m. With 500–1000 m extra uplift above sea level, the upper part of the Shahejie sandstones may be located above sea level, and the distance between the lower part of the Shahejie sandstones to the water level may be less than 1000 m (Fig. 19). The extensive uplift of the Gaoliu area formed a highland relative to other structural belts (eg. Liunan subsag) in the Nanpu Sag, and this altitude difference provided substantial hydraulic drive for penetration of meteoric water into these sandstones (Bjørlykke, 1993). Widely developed faults linked the earth's surface with the sandstone beds in the



**Fig. 19.** Sections restored to different geological time (modified from Zhou, 2000). Note the high land in the Gaoliu area during the uplift period. Note that the burial depth of the Es3 member during the uplift period can be less than 1000 m. The subaerial exposure and developed faults probably can promote meteoric water flux into the Shahejie sandstones.

Shahejie Formation (Fig. 3B) (Li et al., 2010; Zhou, 2000), and served as favorable flow conduits for meteoric freshwater penetration to the studied sandstones. Thus, during the uplift stage (26 Ma–23 Ma), it is very likely that freshwater can be input into the Shahejie sandstones above the lake level and the sandstones with a depth of almost 1000 m below lake level.

In the first burial stage, the Shahejie sandstones experienced compaction with burial depth ranging from about 800 m to approximately 2400 m from the top to the bottom (Fig. 2A). During the initial reburial stage (23–15Ma), the burial depth of the Shahejie Formation was still 300 m shallower than the maximum depth experienced during the first burial stage. The main part of the Shahejie sandstones (ES1–Es<sub>3</sub>) was buried shallower than 1500 m. Stronger compaction should only reoccur when burial depth exceeded the pre-burial depth in the reburial stage, thus, upward compaction drive flow was likely rather weak during the initial reburial stage (23–15 Ma). The widely developed faults linking the earth's surface and the Shahejie sandstone beds (Fig. 3B) remained active from the late Oligocene period to the end of Pliocene period (Li et al., 2010; Zhou, 2000), and possibly served as favorable flow conduits for meteoric freshwater penetration. Considering a combination of these favorable factors, it is likely that the incursion of meteoric water could occur in buried sandstones during the period of 23–15 Ma. After that, freshwater influx would have become slower and pore water would have gradually been modified by ongoing diagenetic reactions in the sandstones. Hydrocarbon emplacement starting around 10 Ma may have also enriched the  $\delta^{18}O_{(SMOW)}$  composition of the pore water, and slowed down the feldspar dissolution reactions to some extent (Marchand et al., 2002). As pore water become relatively limited, quartz overgrowths were precipitated in some deeply buried sandstones, following ongoing feldspar dissolution, which is in consistent with the high  $T_h$  of AFLs in the quartz overgrowths.

5.3. Enhanced secondary pores by burial freshwater leaching

The difference between the amount of feldspar pores and leaching byproducts (kaolinite and quartz cements) obtained from 2D thin sections shows that enhanced porosities (thin section data)

formed by feldspar dissolution in the open Gaoliu sandstone geochemical system can be up to 3%–4.5% (Fig. 20). As 1% thin section porosity accounts for 1.5%–2.0% helium tested porosity (Wang et al., 2013), feldspar dissolution probably enhanced volumetric porosity by up to 5–8%.

The leaching of early-diagenetic calcite cement is evident in some samples (Fig. 6C and D; Fig. 7). Negative linear correlations exist between tested core plug porosity and the amount of carbonate cements in medium-coarse grained sandstones and pebbly sandstones (Fig. 21), indicating that the dissolution of early-diagenetic cement can actually increase reservoir porosity. As burial depth increases, porosity of sandstones with similar amounts of carbonate cements does not decrease (Fig. 21), suggesting that early extensive calcite cementation has effectively retarded compaction, and leaching of such calcite cement released the pore spaces occupied by these cements in the eodiagenetic stage. However, it is difficult to test the amount of these secondary pores formed by calcite leaching using only these thin sections.

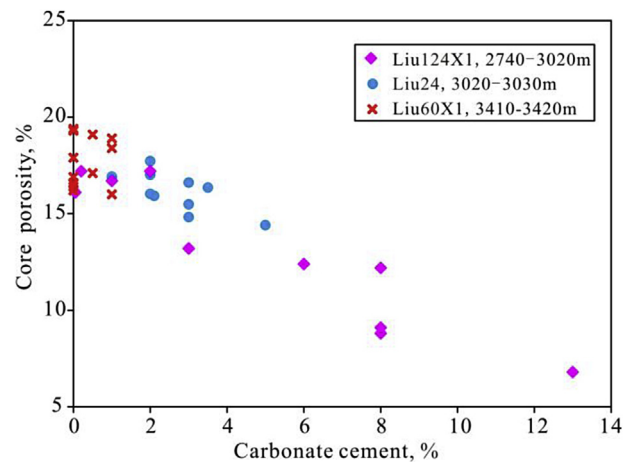


Fig. 21. Relationship between tested core porosity and the amount of carbonate cements in medium-coarse grained sandstones and pebbly sandstones with little clays in three wells.

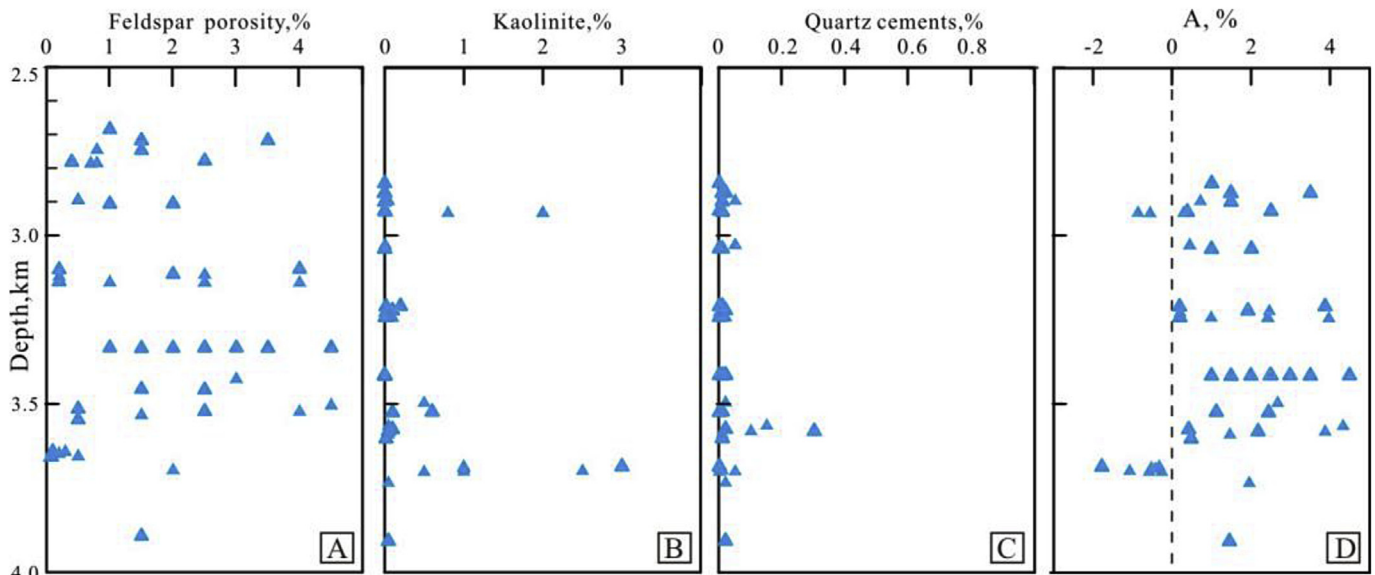


Fig. 20. Vertical variation of the content of feldspar pores, kaolinite and quartz cement and their difference values in thin section in the Gaoliu area (modified from Yuan et al., 2015b). A is the difference between vol % feldspar lost and vol % kaolinite and quartz gained.

With constraints of tested core plug porosity, theoretical porosity-depth trend (compaction curve) from Ramm (1992) (Ramm, 1992) and the amount of enhanced feldspar porosity, secondary porosity formed by leaching of early-diagenetic carbonate cement was estimated. For example, the calculated porosities at a depth of 3000 m and 3500 m were 15% and 12%, respectively. The tested core porosities of sandstones with little clay and calcite cement reach up to 25–28% and 20–22%, respectively (Fig. 22). Then, the porosity differences between tested core porosities and calculated porosity range from 10–13% and 8–10% at depth of 3000 m and 3500 m, respectively. Fluid overpressure does not occur commonly in the studied sandstones, and hydrocarbon emplacement has little impact on porosity of the sandstones with few cement. After deducting the 5–8% porosity generated by feldspar dissolution, the remaining porosity differences (most likely generated by calcite dissolution) are 4–6% at 3000 m and 2–4% at 3500 m, respectively.

Besides the local 200 m of organic-rich mudstones and shales in the lower part of the Shahejie strata, TOC of most other interbedded mudstones in the Shahejie Formations is generally less than 0.5–1.0% (Guo et al., 2013). With the vitrinite reflectance of organic matter ranging from 0.35% to 0.80%, and a mud/sand ratio of 2:1 to 5:1 (Yuan et al., 2015b), the organic CO<sub>2</sub> and organic acids generated from kerogen maturation can account for less than 1–2% secondary pores in the Gaoliu sandstones (Giles and Marshall, 1986; Lundegard et al., 1984). During the uplift period, cooling of hot pore water in the sandstones may dissolve some calcite (Giles and De Boer, 1989). Numerical simulations, however, suggest that the cooling of hot fluids retains a very low capacity for dissolving large amounts of calcite in sandstones (Yuan et al., 2015a). As large volume of meteoric water can provide inorganic CO<sub>2</sub> acid, the meteoric leaching reactions probably can account for the approximated 7–10% enhanced secondary porosities in these sandstones. Thus, meteoric freshwater leaching can improve reservoir quality in an open sandstone geochemical system.

#### 5.4. Summary model for meteoric diagenesis and reservoir-quality evolution pathways

The diagenetic reactions and related reservoir evolution pathways of the studied sandstones in the thick Shahejie Formation beneath the regional unconformity are strongly controlled by the burial-uplift-reburial history and relevant pore water evolution experience in the rocks (Fig. 23).

During the first burial stage, the sandstones in the Shahejie Formation were buried to the depth from approximately 800 m–2400 m. With the impact of alkaline connate lake water, eodiagenetic reactions including compaction and early calcite cementation dominated the physical and chemical alterations in the sandstones, and porosity and permeability of the sandstones were reduced significantly in such a period.  $\delta^{18}\text{O}_{(\text{SMOW})}$  composition of the pore water was gradually elevated as chemical diagenesis continued. Feldspar leaching with some kaolinite precipitation likely occurred in the sandstones at the bottom of the Shahejie Formation, in conjunction with an influx of fluids charged with organic acids (CO<sub>2</sub>) from the kerogen thermal maturation in source-rocks.

During the uplift and initial reburial stages, great uplift occurred. The upper part of the Shahejie sandstones could be located above sea (lake) water level, and the distance from the lower part of the Shahejie sandstones to the lake level could be less than 1000 m. Meteoric freshwater was injected into the Shahejie sandstone beds from the unconformity (the earth's surface), with faults connecting the earth's surface and the sandstone beds serving as flow paths. With a large amount of meteoric flux, extensive dissolution of feldspars and calcite minerals occurred without the precipitation of secondary minerals, leading to significantly enhanced porosity and permeability. Stronger compaction did not occur because reburial depth did not exceed pre-burial depth.  $\delta^{18}\text{O}_{(\text{SMOW})}$  composition of pore water decreased dramatically with freshwater flux. As the present burial depths of such

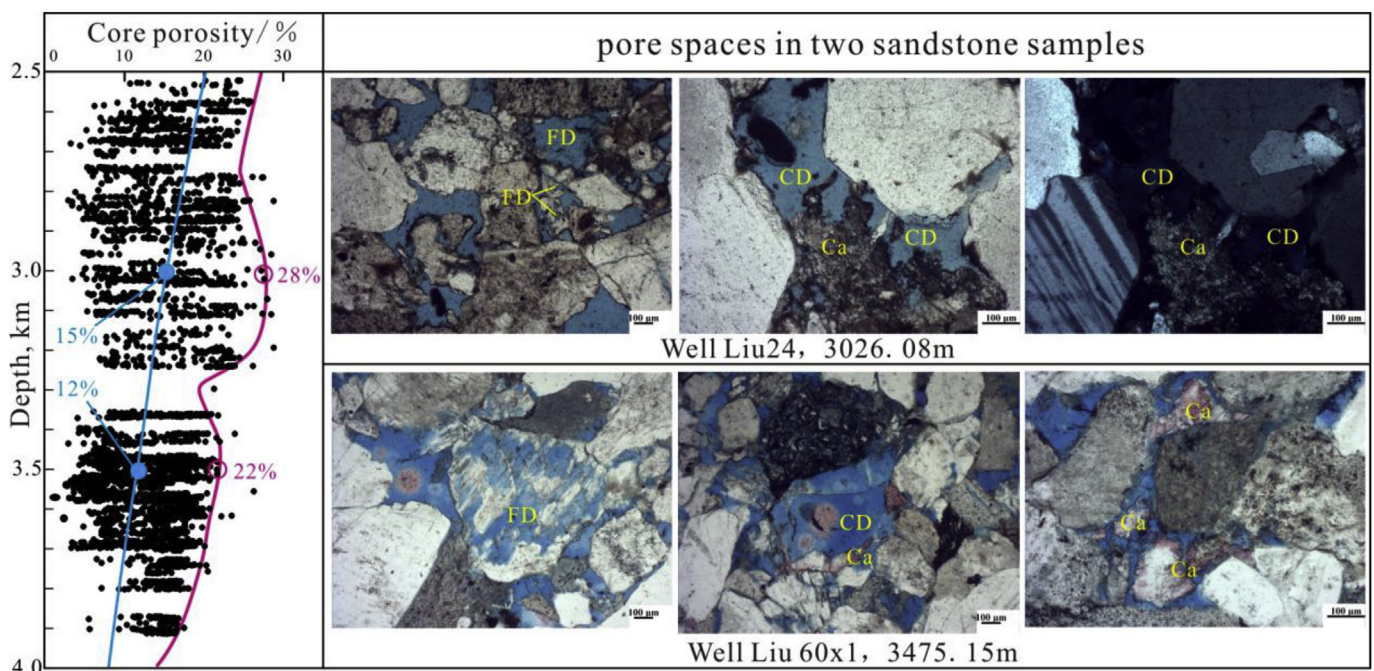


Fig. 22. Tested core porosities and calculated porosity curve with a theoretical equation from Ramm (1992). The equation is  $\phi = 45e[-(0.23 + 0.27\text{CFGR})z]$ , where CFGR represent the clay content in sandstones,  $z$  represents the burial depth. FD: secondary pore formed by feldspar dissolution, CD: secondary pore formed by dissolution of calcite cement, Ca: remnant leached calcite cement.

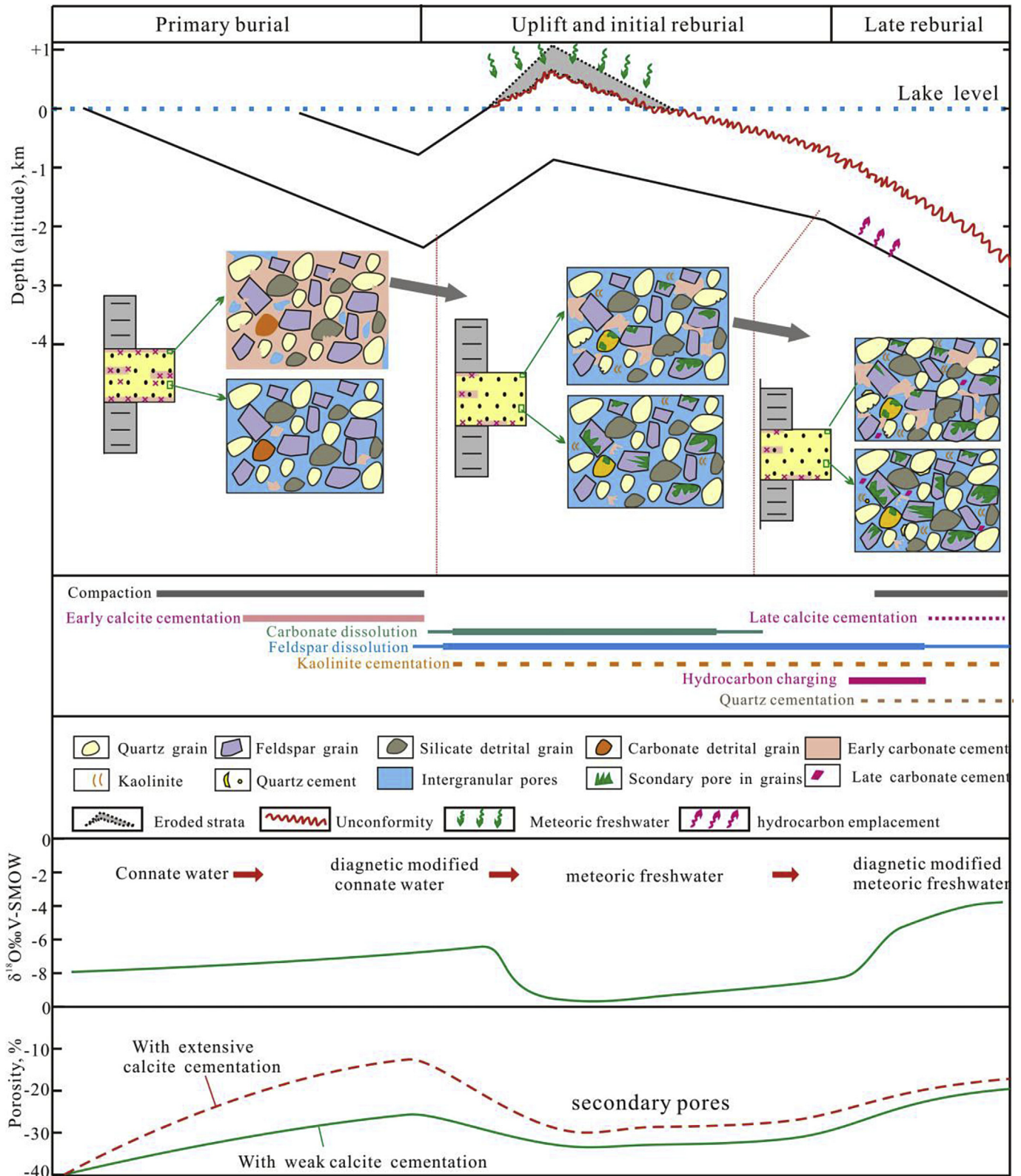


Fig. 23. Evolution of meteoric relevant diagenesis and reservoir-quality in the Shehejie sandstones in the Gaoliu area, Nanpu Sag, Bohai Bay Basin.

sandstones are greater than 3500–4000 m, it seems that “deep” incursion of meteoric freshwater occurred in such sandstones.

During the late reburial stage, stronger compaction occurred when burial depth exceeded the pre-burial depth. Feldspar dissolution continued without extensively on-going meteoric water flux, but with precipitation of some quartz, kaolinite, and a few late-diagenetic calcite cements. Porosity and permeability were reduced to some extent by quick and deep burial processes during this period, though feldspar dissolution may enhance some physical properties.  $\delta^{18}\text{O}_{(\text{SMOW})}$  composition of pore water was elevated with by continuing diagenetic reactions. Hydrocarbon charging around 10 Ma may also have enriched the  $\delta^{18}\text{O}_{(\text{SMOW})}$  composition, and the hydrocarbon emplacement may also slowed down the chemical diagenetic reactions to some extent.

### 5.5. Significance

Globally, most studies suggest that meteoric freshwater leaching reaction generally occurs in sandstones at relatively shallow depth after deposition or directly beneath an unconformity (generally < 200 m) during the uplift stage (Emery et al., 1990; Huang et al., 2003). To the present, secondary pores in most deeply buried sandstones in the Shahejie Formation in the Bohai Bay Basin have been suggested to be formed by burial leaching reactions induced by carbonic acid and (or) organic acids from kerogen in source rocks (Gao et al., 2016; Yongshi et al., 2016; Yuan and Wang, 2001; Zhang et al., 2014; Zhu et al., 2014).

This study, however, demonstrates that freshwater incursion did have occurred in the deeply buried Shahejie sandstones in the Gaoliu area and have formed large amounts of enhanced secondary porosity in these sandstones to improve the reservoir quality. These results indicate that meteoric freshwater leaching reactions cannot be ignored even in deep layers in petroliferous basins. With combination of great uplift and faults connecting the sandstone beds and the earth's surface, the meteoric leaching reactions in the sandstones can significantly extend the effective depth range for hydrocarbon exploration.

## 6. Conclusion

- (1) The Shahejie sandstones in the Gaoliu area, Nanpu Sag experienced compaction and calcite cementation in the initial burial stage, dissolution of calcite and feldspars in the uplift and initial reburial stages, and feldspar dissolution, in conjunction with kaolinite and quartz cementation and late-diagenetic calcite cementation in the late reburial stage.
- (2) The uplift that occurred during the late Oligocene period made the upper part of the Shahejie sandstones located above lake level and the lower part of the Shahejie sandstones close to lake level (although far from the unconformity). During the uplift and initial reburial stages, the significant uplift and the widely developed faults connecting the earth's surface promoted the meteoric freshwater flux into the sandstone beds in the thick Shahejie Formation beneath the regional conformity. At present, it seems that meteoric freshwater occurred in deep buried sandstones regardless of the great uplift.
- (3) Petrography texture and tested core porosity data suggest that the meteoric freshwater leaching reactions in the Shahejie sandstones in the Gaoliu area enhanced abundant secondary porosity by effectively removing the dissolved solutes out of the sandstones.
- (4) Freshwater incursion can occur in subsurface sandstones located deep beneath an unconformity, with great uplift moving these sandstones above or close to sea (lake) level

and with faults connecting the earth's surface and the sandstone beds. Meteoric freshwater leaching reactions cannot be ignored in deep layers in petroliferous basins with such geological background.

## Acknowledgments

This study was financially supported by the Natural Science Foundation of China Project (No. U1262203, No. 41602138), a National Science and Technology Special Grant (No. 2016ZX05006-007), China Postdoctoral Science Foundation funded project (2015M580617), and Shandong Post doctoral innovation project (201502028). Jidong Oilfield Company of PetroChina is thanked for supplying all rock samples, blue epoxy resin-impregnated thin sections and some geological data. Doubly polished sections were prepared by Ian Chaplin in Durham University. Petrography and fluid inclusion analysis were made in State key laboratory in China University of Petroleum. Sample preparation and SMIS analysis were assisted by staffs in IGGCAS. Professor Andrew Aplin in Durham University and Keyuliu in China University of Petroleum provided constructive suggestion for this manuscript. Two anonymous reviewers are thanked for their constructive comments to the primary manuscript.

## References

- Aplin, A.C., Warren, E.A., 1994. Oxygen isotopic indications of the mechanisms of silica transport and quartz cementation in deeply buried sandstones. *Geology* 22 (9), 847–850.
- Baruch, E.T., Kennedy, M.J., Löhr, S.C., Dewhurst, D.N., 2015. Feldspar dissolution-enhanced porosity in Paleoproterozoic shale reservoir facies from the Barney Creek Formation (McArthur Basin, Australia). *AAPG Bull.* 99 (9), 1745–1770.
- Bjørlykke, K., 1998. Clay mineral diagenesis in sedimentary basins — a key to the prediction of rock properties. Examples from the North Sea Basin. *Clay Miner.* 33 (1), 15–34.
- Bjørlykke, K., 1993. Fluid flow in sedimentary basins. *Sediment. Geol.* 86 (1–2), 137–158.
- Bjørlykke, K., Jahren, J., 2012. Open or closed geochemical systems during diagenesis in sedimentary basins: constraints on mass transfer during diagenesis and the prediction of porosity in sandstone and carbonate reservoirs. *AAPG Bull.* 96 (12), 2193–2214.
- Bjørlykke, K., Aagaard, P., 1992. Clay Minerals in North Sea Sandstones: in *Origin, Diagenesis and Petrophysics of Sandstones*, vol. 47. SEPM Special Publications, pp. 65–80.
- Chen, Y., Steele-Macinnis, M., Ge, Y., Zhou, Z., Zhou, Y., 2016. Synthetic saline-aqueous and hydrocarbon fluid inclusions trapped in calcite at temperatures and pressures relevant to hydrocarbon basins: a reconnaissance study. *Mar. Pet. Geol.* 76, 88–97.
- Chuhan, F.A., Bjørlykke, K., Lowrey, C.J., 2001. Closed-system burial diagenesis in reservoir sandstones: examples from the Garn Formation at Haltenbanken area, offshore mid-Norway. *J. Sediment. Res.* 71 (1), 15–26.
- Clayton, R.N., Friedman, I., Graf, D.L., Mayeda, T.K., Meents, W.F., Shimp, N.F., 1966. The origin of saline formation waters: 1. Isotopic composition. *J. Geophys. Res.* 71 (16), 3869–3882.
- Dong, Y.X., Wang, Z.C., Zheng, H.J., Xu, A.N., 2008. Control of strike-slip faulting on reservoir formation of oil and gas in Nanpu sag. *Pet. Explor. Dev.* 35 (4), 424–430.
- Dutton, S.P., Loucks, R.G., 2010. Diagenetic controls on evolution of porosity and permeability in lower Tertiary Wilcox sandstones from shallow to ultradeep (200–6700m) burial, Gulf of Mexico Basin, U.S.A. *Mar. Pet. Geol.* 27 (1), 69–81.
- Emery, D., Myers, K.J., Young, R., 1990. Ancient subaerial exposure and freshwater leaching in sandstones. *Geology* 18 (12), 1178–1181.
- Fayek, M., Harrison, T.M., Grove, M., Mckeegan, K.D., Coath, C.D., Boles, J.R., 2001. In situ stable isotopic evidence for protracted and complex carbonate cementation in a petroleum reservoir, North Coles Levee, San Joaquin Basin, California, U.S.A. *J. Sediment. Res.* 71 (3), 444–458.
- França, A.B., Araújo, L.M., Maynard, J.B., Potter, P.E., 2003. Secondary porosity formed by deep meteoric leaching: Botucatu eolianite, southern South America. *AAPG Bull.* 87 (7), 1073–1082.
- Friedman, I., O'Neil, J.R., 1977. *Data of Geochemistry: Compilation of Stable Isotope Fractionation Factors of Geochemical Interest [M]*. US Government Printing Office.
- Gao, Y., Zhang, J., Li, H., Yu, X., 2016. Diagenesis and porosity evolution of deep  $\text{E}_3^{2+3}$  formation in Gaoshangpu Oilfield, Nanpu Sag. *Fault-Block Oil Gas Field* 23 (6), 703–708.
- Giles, M.R., Marshall, J.D., 1986. Constraints on the development of secondary

- porosity in the subsurface: re-evaluation of processes. *Mar. Pet. Geol.* 3 (3), 243–255.
- Giles, M.R., De Boer, R.B., 1989. Secondary porosity: creation of enhanced porosities in the subsurface from the dissolution of carbonate cements as a result of cooling formation waters. *Mar. Pet. Geol.* 6 (3), 261–269.
- Giles, M.R., De Boer, R.B., 1990. Origin and significance of redistributive secondary porosity. *Mar. Pet. Geol.* 7 (4), 378–397.
- Girard, J., Munz, I.A., Johansen, H., Hill, S., Canham, A., 2001. Conditions and timing of quartz cementation in Brent reservoirs, Hild Field, North Sea: constraints from fluid inclusions and SIMS oxygen isotope microanalysis. *Chem. Geol.* 176 (1–4), 73–92.
- Gluyas, J.G., Robinson, A.G., Primmer, T.P., 1997. *Rotliegende Sandstone Diagenesis: a Tale of Two Waters*. Geofluids II, Belfast, pp. 291–294.
- Guo, Y., Pang, X., Dong, Y., Jiang, Z., Chen, D., Jiang, F., 2013. Hydrocarbon generation and migration in the Nanpu Sag, Bohai Bay Basin, eastern China: insight from basin and petroleum system modeling. *J. Asian Earth Sci.* 77, 140–150.
- Harwood, J., Aplin, A.C., Fialips, C.I., Iliffe, J.E., Kozdon, R., Ushikubo, T., Valley, J.W., 2013. Quartz cementation history of sandstones revealed by high-resolution SIMS oxygen isotope analysis. *J. Sediment. Res.* 83 (7), 522–530.
- Higgs, K.E., Zwingmann, H., Reyes, A.G., Funnell, R.H., 2007. Diagenesis, porosity evolution, and petroleum emplacement in tight gas reservoirs, Taranaki Basin, New Zealand. *J. Sediment. Res.* 77 (12), 1003–1025.
- Huang, S.J., Wen-Hui, W.U., Jie, L., Shen, L.C., Huang, C.G., 2003. Generation of secondary porosity by meteoric water during time of subaerial exposure: an example from Yanchang Formation sandstone of Triassic of Ordos Basin. *Earth Sci. — J. China Univ. Geosci.* 28 (4), 419–424.
- Li, H., Jiang, Z., Dong, Y., Wang, X., Qi, L., 2010. Control of faults on hydrocarbon migration and accumulation in Nanpu Sag, Bohai Bay Basin. *Geoscience* 24 (4), 755–761.
- Li, X., Tang, G., Gong, B., Yang, Y., Hou, K., Hu, Z., Li, Q., Liu, Y., Li, W., 2013. Qinghu zircon: A working reference for microbeam analysis of U-Pb age and Hf and O isotopes. *Chin. Sci. Bull.* 58 (36), 4647–4654.
- Li, X., Li, Z., He, B., Li, W., Li, Q., Gao, Y., Wang, X., 2012. The Early Permian active continental margin and crustal growth of the Cathaysia Block: in situ U-Pb, Lu-Hf and O isotope analyses of detrital zircons. *Chem. Geol.* 328, 195–207.
- Lundegard, P.D., Land, L.S., Galloway, W.E., 1984. Problem of secondary porosity: Frio Formation (Oligocene), Texas Gulf Coast. *Geology* 12 (7), 399–402.
- Mansurbeg, H., El-ghali, M.A.K., Morad, S., Plink-Björklund, P., 2006. The impact of meteoric water on the diagenetic alterations in deep-water, marine siliciclastic turbidites. *J. Geochem. Explor.* 89 (1–3), 254–258.
- Marchand, A.M.E., Macaulay, C.I., Haszeldine, R.S., Fallick, A.E., 2002. Pore water evolution in oilfield sandstones: constraints from oxygen isotope microanalyses of quartz cement. *Chem. Geol.* 191 (4), 285–304.
- Méheut, M., Lazzari, M., Balan, E., Mauri, F., 2007. Equilibrium isotopic fractionation in the kaolinite, quartz, water system: prediction from first-principles density-functional theory. *Geochim. Cosmochim. Acta* 71 (13), 3170–3181.
- Molenaar, N., Felder, M., Bär, K., Götz, A.E., 2015. What classic greywacke (litharenite) can reveal about feldspar diagenesis: An example from Permian Rotliegend sandstone in Hessen, Germany. *Sediment. Geol.* 326, 79–93.
- Ramm, M., 1992. Porosity-depth trends in reservoir sandstones: theoretical models related to Jurassic sandstones offshore Norway. *Mar. Pet. Geol.* 9 (5), 553–567.
- Schmidt, V., McDonald, D.A., 1979. The Role of Secondary Porosity in the Course of Sandstone Diagenesis, vol. 26. SPEM Special Publication, pp. 175–207.
- Song, X., Liu, X., Xia, J., Yu, J., Tang, C., 2006. A study of interaction between surface water and groundwater using environmental isotope in Huaisha River basin: Science in China Series D. *Earth Sci.* 49 (12), 1299–1310.
- Sun, S., Xie, J., Li, G., Qiu, C., 1982. Hydrogen and oxygen isotopic composition and genesis of the ground water in Jizhong depression (in Chinese with English abstract). *Oil Gas Geol.* 3 (3), 240–250.
- Surdam, R.C., Boese, S.W., Crossey, L.J., 1984. The Chemistry of Secondary porosity. AAPG Mem. 37 (2), 183–200.
- Taylor, T.R., Land, L.S., 1996. Association of allochthonous waters and reservoir enhancement in deeply buried Miocene sandstones: Picaroon field, Corsair trend, offshore Texas. In: Crossey, L.J., Loucks, R., Totten, M.W. (Eds.), *Siliciclastic Diagenesis and Fluid Flow: Concepts and Applications*, vol. 55. SEPM Special Publication, pp. 37–48.
- Thyne, G., 2001. A model for diagenetic mass transfer between adjacent sandstone and shale. *Mar. Pet. Geol.* 18 (6), 743–755.
- Wang, L.Z., Dai, T.M., Peng, P., 2005.  $^{40}\text{Ar}/^{39}\text{Ar}$  dating of diagenetic illites and its application in timing gas emplacement in gas reservoirs. *Earth Sci.-J. China Univ. Geosci.* 30 (1), 78–82.
- Wang, Y., Cao, Y.C., Xi, K.L., Song, G., Liu, H.M., 2013. A recovery method for porosity evolution of clastic reservoirs with geological time: a case study from the upper submember of Es4 in the Dongying depression, Jiayang subbasin (In Chinese with English abstract). *Acta Petrol. Sin.* 34 (6), 1100–1111.
- Wilkinson, M., Milliken, K.L., Haszeldine, R.S., 2001. Systematic destruction of K-feldspar in deeply buried rift and passive margin sandstones. *J. Geol. Soc.* 158 (4), 675–683.
- Wilkinson, M., Haszeldine, R.S., Morton, A., Fallick, A.E., 2014. Deep burial dissolution of K-feldspars in a fluvial sandstone, Pentland Formation, UK Central North Sea. *J. Geol. Soc.* 171 (5), 635–647.
- Wood, J.R., Hewett, T.A., 1982. Fluid convection and mass transfer in porous sandstones—a theoretical model. *Geochim. Cosmochim. Acta* 46 (10), 1707–1713.
- Yongshi, W., Yong, W., Deshun, Z., Juhong, D., Bing, S., Jiajun, Z., 2016. Genetic mechanism of high-quality glutenite reservoirs at the steep slope in northern Dongying. *China Pet. Explor.* 21 (2), 28–36.
- Yuan, G.H., 2015. Genetic Mechanism of Dissolution of Feldspars and Carbonate Minerals during Diagenesis and Its Impact on Reservoir Poroperm (In Chinese with English Abstract). Ph.D. thesis. China University of Petroleum (East China), Qingdao, China, 166 pp.
- Yuan, G., Cao, Y., Jia, Z., Gluyas, J., Yang, T., Wang, Y., Xi, K., 2015a. Selective dissolution of feldspars in the presence of carbonates: the way to generate secondary pores in buried sandstones by organic  $\text{CO}_2$ . *Mar. Pet. Geol.* 60, 105–119.
- Yuan, G., Cao, Y., Gluyas, J., Li, X., Xi, K., Wang, Y., Jia, Z., Sun, P., Oxtoby, N.H., 2015b. Feldspar dissolution, authigenic clays, and quartz cements in open and closed sandstone geochemical systems during diagenesis: typical examples from two sags in Bohai Bay Basin, East China. *AAPG Bull.* 99 (11), 2121–2154.
- Yuan, G., Gluyas, J., Cao, Y., Oxtoby, N.H., Jia, Z., Wang, Y., Xi, K., Li, X., 2015c. Diagenesis and reservoir quality evolution of the Eocene sandstones in the northern Dongying Sag, Bohai Bay Basin, East China. *Mar. Pet. Geol.* 62, 77–89.
- Yuan, J., Wang, Q.Z., 2001. Distribution and generation of deep reservoir secondary pores, Paleogene, Dongying Sag (In Chinese with English abstract). *J. Petrol.* 21 (1), 43–47.
- Zhang, Q., Zhu, X., Steel, R.J., Zhong, D., 2014. Variation and mechanisms of clastic reservoir quality in the Paleogene Shahejie Formation of the Dongying Sag, Bohai Bay Basin, China. *Pet. Sci.* 11, 200–210.
- Zhang, W.C., Li, H., Li, H.J., Meng, Y.L., Yang, F.B., 2008. Genesis and distribution of secondary porosity in the deep horizon of Gaoliu area, Nanpu Sag. *Pet. Explor. Dev.* 35 (3), 308–312.
- Zhou, H., 2000. Relationship between formation, evolution, and hydrocarbon in Nappu Sag (in Chinese with English abstract). *Oil Gas Geol.* 21 (4), 345–349.
- Zhu, C., Blum, A.E., Veblen, D.R., Wanty, R.B., Seal, R., 2004. Feldspar Dissolution Rates and Clay Precipitation in the Navajo Aquifer at Black Mesa, vol. 1. A.A. Balkema, Arizona, USA, pp. 441–442.
- Zhu, C., Lu, P., Zheng, Z., Ganor, J., 2010. Coupled alkali feldspar dissolution and secondary mineral precipitation in batch systems: 4. Numerical modeling of kinetic reaction paths. *Geochim. Cosmochim. Acta* 74 (14), 3963–3983.
- Zhu, G., Zhang, S., Wang, Y., Wang, Z., 2011. Forming condition and enrichment mechanism of the Nanpu Oilfield in the Bohai Bay Basin, China. *Acta Geol. Sin.* 85 (1), 97–113.
- Zhu, X., Wu, D., Zhang, X., Wang, X., 2014. Genesis of low permeability reservoirs of the nearshore subaqueous fan in Shahejie Formation in Dongying sag, Bohai Bay Basin. *Oil Gas Geol.* 35 (5), 646–653.